Validation of Ionospheric Models
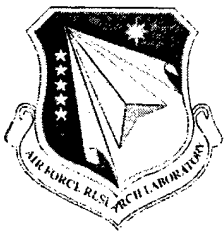
Dwight T. Decker
Patricia H. Doherty
Neil J. Grossbard

Boston College
Institute for Scientific Research
Chestnut Hill, MA 02467

31 March 1998

20030822 074

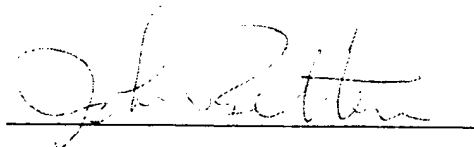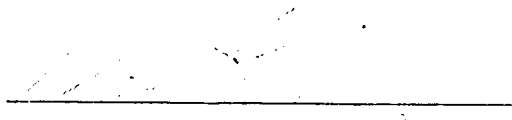**AIR FORCE RESEARCH LABORATORY**
Space Vehicles Directorate
29 Randolph Rd
AIR FORCE MATERIEL COMMAND
Hanscom AFB, MA 01731-3010

This technical report has been reviewed and is approved for publication.

_____   _____
Contract Manager   Branch Chief

* (This report has been reviewed by the ESC Public Affairs Office (ESC/PAM) and is releasable to the National Technical Information Service (NTIS).)

Qualified requestors may obtain additional copies from the Defense Technical Information Center (DTIC). * (All others should apply to the NTIS.)

If your address has changed, or if you wish to be removed from the mailing list, or if the addressee is no longer employed by you, please notify AFRL/VSIM, 29 Randolph Road, Hanscom AFB, MA 01731-3010. This will help us to maintain a current mailing list.

DO NOT RETURN COPIES OF THIS REPORT unless contractual obligations or notices on a specific document require that it be returned.

REPORT DOCUMENTATION PAGE

1. AGENCY USE ONLY (Leave blank)	2. REPORT DATE 31 March 1998	3. REPORT TYPE AND DATES COVERED Scientific Report No. 2

4. TITLE AND SUBTITLE

VALIDATION OF IONOSPHERIC MODELS

5. FUNDING NUMBERS

Contract:
F19628-96-C-0039
PE 61102F
PR 1010
TA IM
WU AC

6. AUTHOR(S)

Dwight T. Decker
Patricia H. Doherty
Neil J. Grossbard

7. PERFORMING ORGANIZATION NAME(S) AND ADDRESS(ES)

Boston College
Institute for Scientific Research
140 Commonwealth Avenue
Chestnut Hill, MA 02167-3862

8. PERFORMING ORGANIZATION REPORT NUMBER

9. SPONSORING / MONITORING AGENCY NAME(S) AND ADDRESS(ES)

Air Force Research Laboratory
29 Randolph Road
Hanscom AFB, MA 01731-3010
Contract Manager: John Retterer/VSBP

10. SPONSORING / MONITORING AGENCY REPORT NUMBER

AFRL-VS-HA-TR-98-0126

11. SUPPLEMENTARY NOTES

12a. DISTRIBUTION / AVAILABILITY STATEMENT

Approved for public release; distribution unlimited.

12b. DISTRIBUTION CODE

13. ABSTRACT (Maximum 200 words)

The objective of this research is to obtain various ionospheric measurements from a wide range of geographic locations and to utilize the resulting databases to validate the theoretical ionospheric models that are the basis of the Parameterized Real-time Ionospheric Specification Model (PRISM) and the Ionospheric Forecast Model (IFM). Thus, our various efforts can be generally categorized as either modeling studies or work concerning observational databases.

14. SUBJECT TERMS
Ionospheric weather, global F-region modeling, total electron content (TEC), GPS, GPS/MET, occultations, plasma structure, blobs

15. NUMBER OF PAGES

16. PRICE CODE

17. SECURITY CLASSIFICATION OF REPORT UNCLASSIFIED	18. SECURITY CLASSIFICATION OF THIS PAGE UNCLASSIFIED	19. SECURITY CLASSIFICATION OF ABSTRACT UNCLASSIFIED	20. LIMITATION OF ABSTRACT SAR

1. INTRODUCTION

The objective of this research is to obtain various ionospheric measurements from a wide range of geographic locations and to utilize the resulting databases to validate the theoretical ionospheric models that are the basis of the Parameterized Real-time Ionospheric Specification Model (PRISM) and the Ionospheric Forecast Model (IFM). Thus, our various efforts can be generally categorized as either modeling studies or work concerning observational databases.

2. MODELING STUDIES

2.1. Boundary and Subauroral Blobs

In earlier work using a first principles theoretical model, we successfully simulated the production of boundary blob type structures [*Anderson et al.,* 1996]. However, these boundary blob simulations were not made with any particular observations in mind. We simply produced blob-like features in the evening sector at auroral latitudes. Ideally, if a database of blob observations were available that described the seasonal and UT morphology of blobs, we could then perform a series of simulations to determine if the mechanism used for producing blobs (solar produced plasma and time varying convection) is capable of producing blobs with the correct morphology. Unfortunately, such a blob database is unavailable so we chose to attempt to simulate blobs as seen in particular observations. The point of such calculations was not to model the precise details of the particular observations because we do not know the details of the time varying convection during any of the periods considered. Rather, our purpose was to demonstrate that solar produced plasma and time varying convection are capable of producing blobs at some of the times and locations that they are observed.

With this in mind, we performed a simulation for 29 January 1979, a day when the Chatanika radar observed a series of blobs from just before 19 CGLT to just before 01 CGLT. This attempt involved modifying our original simulation in two ways. First, our variation of the convection pattern was shifted in UT so it would have the potential of producing blobs at the appropriate time. Second, we shifted from December solstice to 29 January. Both of these changes were crucial. The shift away from solstice was crucial for allowing high-density plasma to be transported from the daytime across the polar cap into the auroral regions at the appropriate time. The shift in time of when the convection pattern was varied ensured that this plasma was directed at the appropriate time into the evening sector. The resultant blobs appeared at the appropriate time and were comparable in magnitude to what was actually seen in the experiment. However, the blobs were at somewhat higher latitudes than what was observed on that particular day.

Our next series of simulations were designed to produce blobs across the entire field of view of the Chatanika radar. They involved changing Hairston/Heelis patterns consistent with assumed changes in the IMF B_y, but the timing and duration of these changes were varied as well as the precise size and location of the patterns. We found that it was relatively straightforward to produce a series of blobs in the vicinity of Chatanika during this local time period. In Figure 1, we show an example of a simulated radar scan very similar to those seen on 29 January. Figure 2
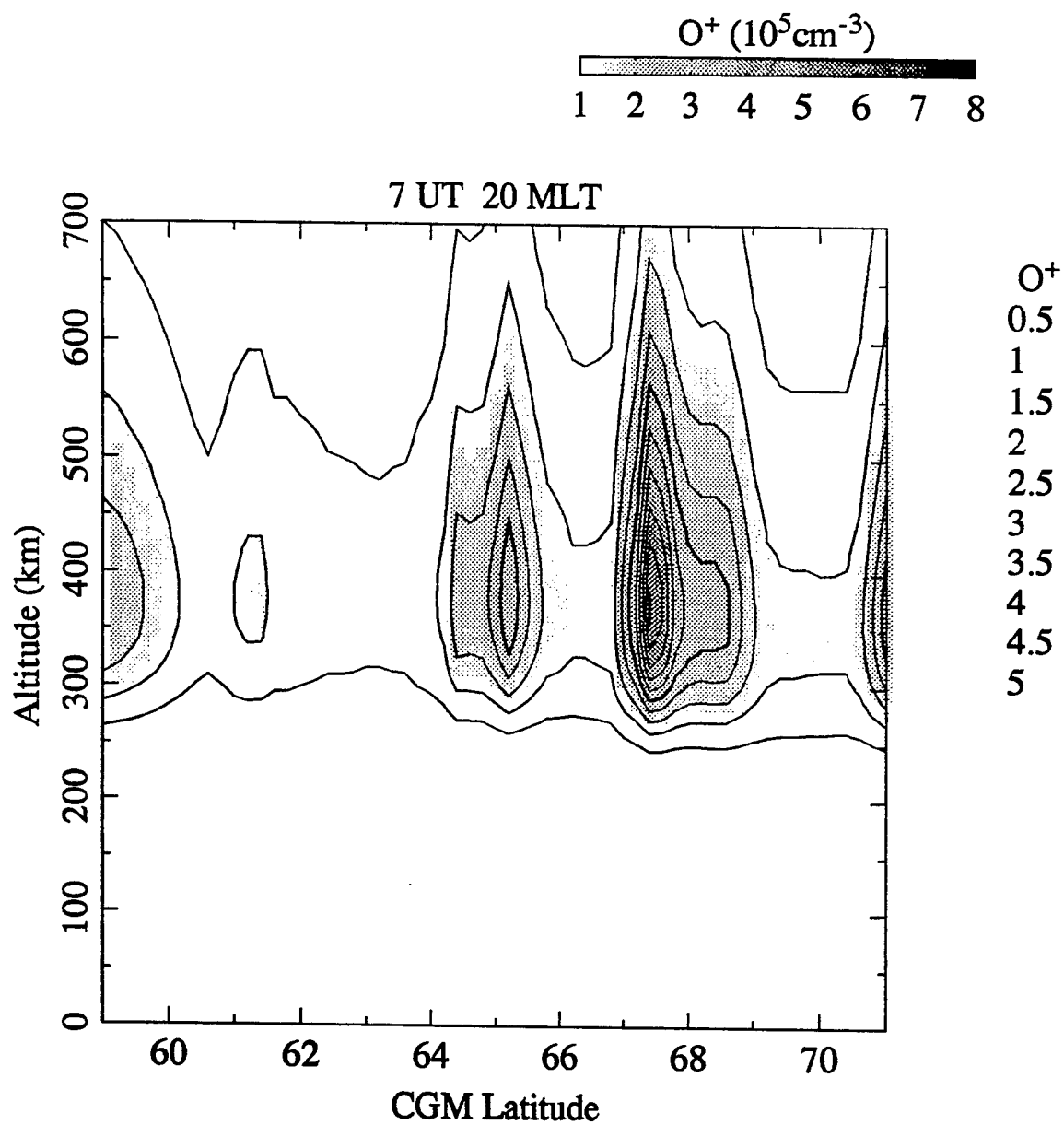
FIGURE 1. Simulated Radar Scan

shows the location of both the Chatanika observed blobs and the simulated blobs. The circles are the locations of the center of the observed F region boundary and sub-auroral blobs. The asterisks are the center locations of the simulated blobs. The time variation consists of going from a positive B_y pattern (8 gamma) to a negative B_y pattern (-8 gamma) and back to positive. In this case, the first switch to -8 gamma was at 02 UT followed by the return to positive B_y at 0330 UT. Another switch to negative and back to positive was made at 0730 and 0830 respectively, with a final set of switches at 1000 and 1030. The initial switches at 0200 UT and 0330 UT are responsible for the blobs seen at 1900 - 2100 mlt as well as the blobs seen equatorward of the observed subauroral blobs at 2200 - 0000 mlt. Note that Chatanika is at 1900 MLT at around 6 UT. So the blobs seen at 1900 MLT (6 UT) are the result of B_y switches that occurred 4 and 2.5 hours earlier. The more poleward blobs are the result of the later switches in the patterns. Also the patterns prior to 0730 UT used a 15° polar cap radius and after 0730 UT the radius was 12°. The cross cap potential was 80 kV for the entire simulation. Our original blob simulation used the 12° radius and 80 kV potential.

The point to reiterate is that we know little about the actual convection on that day, and so we cannot really say that we have modeled this particular day in detail. Rather these simulations illustrate that solar produced plasma and time varying convection are capable of producing blobs at the times and locations that they are observed. Given our success modeling this one Chatanika case [*Weber et al.,* 1985]; we have performed simulations of two more Chatanika cases, a couple of Eiscat cases, and one case where observations were available at three radar sites (Eiscat, Chatanika, and Millstone). The goal continued to be the same; that, is not to model the details of a particular day by using day specific convection, but to produce features similar to what were seen on a given day.

The two Chatanika cases were for 27 February 1980 [*Vickrey et al.,* 1980] and 11 November 1981 [*Rino et al.,* 1983]. In both cases blob like structures were seen through much of the night at latitudes near Chatanika. We performed simulations that again involved changing Hairston/Heelis convection patterns consistent with assumed changes in the IMF B_y. The timing and duration of these changes were similar to what was done in our earlier simulations. Blob-like features were produced that were qualitatively similar to what was seen by the radar in both cases. The two Eiscat cases were for 25 February 1984 [*Tsunoda et al.,* 1985] and 2 October 1991 [*Pryse et al.,* 1996]. In both of these cases, blobs were seen at nighttime and the simulations produced blobs at the appropriate times in the Eiscat region by again using B_y driven changes of Hairston/Heelis convection patterns. Finally, a case involving three radars (Eiscat, Chatanika, and Millstone) was studied [*de la Beaujardiere et al.,* 1985]. Blobs were observed at night at all three radars (17-19 November 1981), but a strong UT dependence was seen in the magnitude of the electron density around local midnight. In simulating this period we used a IMF driven Weimer convection pattern for Millstone and B_y driven changes to Hairston/Heelis patterns for Eiscat and Chatanika. We believe this is a reasonable approach because the radars were compared at the same local times, which means the various observations did not take place at the same UT times. Thus, it is not necessary to use the same convection patterns in simulating what was seen at the different radars. The simulations produce blobs and, in agreement with observation, show Eiscat having much larger densities than Chatanika or north of Millstone. However, observations also indicate that Chatanika has larger densities than those seen north of Millstone, but the simulations produce similar densities at Chatanika and north of
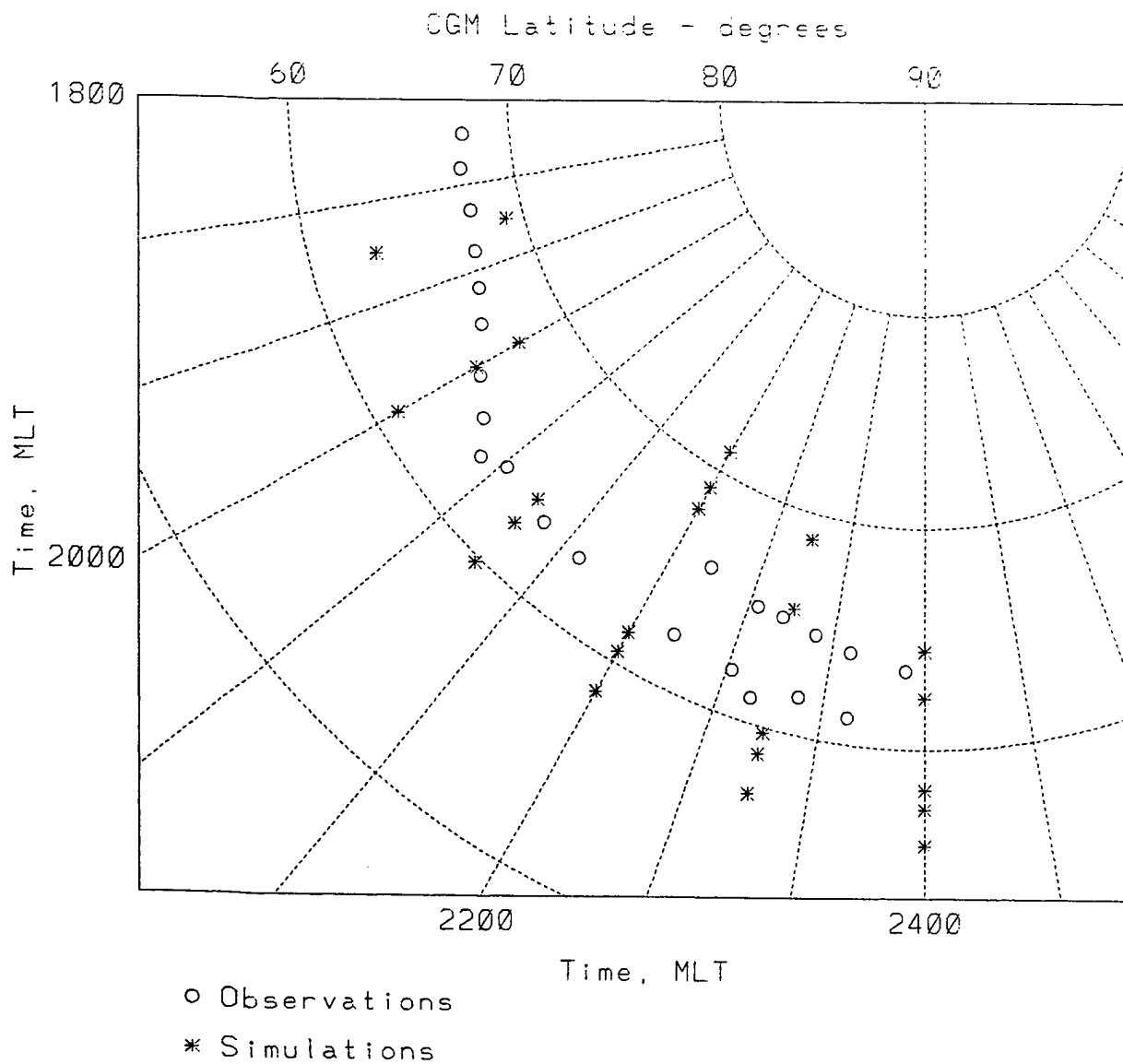
FIGURE 2. Location of Chantanika Observed Blobs and Simulated Blobs

Millstone. Of course, what would be particularly interesting in this case would be to have day specific convection. There is some IMF data available so a future project could be to simulate this entire period with event driven Weimer potentials.

2.2. Modeled Patches/Blobs and Scintillation Observations

As stated above, one approach to validating our high latitude modeling would be to focus not on individual days but on observed blob climatology. However as also mentioned, we know of no assembled data set that gives the complete seasonal and UT morphology of blobs. A similar situation holds for polar cap patches, but one way around this problem that has been tried before was to compare the seasonal and UT variations of 250-MHz intensity scintillation observations made at Thule, Greenland with simulated polar cap patch morphology [*Basu et al.*, 1995]. Inspired by this example, we have compared 250-MHz intensity scintillation observations made at Sondrestrom, Greenland to a series of simulations designed to produce patches and blobs at night (20 to 8 UT) in the vicinity of Sondrestrom. This has been done for December 1991, March 1992, and June 1992. We found that no single simulation would produce the observed monthly behavior. This was because the particular details of the time-varying convection used in a simulation would determine when and where the patches and blobs were produced. However, by performing a series of simulations with different time-varying convection patterns and plotting the results together, we produced a seasonal and UT behavior that is remarkably similar to the behavior of the observed scintillations.

In Figure 3, we show the percent occurrence of intensity scintillations for December 1991 (>8 dB) at 250 MHz observed at Sondrestrom as a function of UT (the solid curve). Note that the vertical scale is given on the right edge of the plot. The six dotted curves are from six sets of various simulations. Each dotted curve is from a set of 14 simulations that used similar variations in convection pattern. For example, in one set, the convection pattern was switched from B_y positive to negative and back again with the switch back to positive occurring 1 hour before the time being considered at Sondrestrom. So if we are interested in what is at Sondrestrom at 1930 UT, then the first switch is at 1700 and the second switch is at 1830, 1 hour before 1930. Other sets of runs considered different times between the switch back to positive and the time at Sondrestrom. One set oscillated B_y every half an hour and another set changed between $B_y = -8$ and 0 gamma rather than -8 and +8 gamma. Each individual simulation produced three high-resolution cuts around Sondrestrom at a particular UT (1930 - 0830). What is plotted is the maximum density at 350 km in a 4.4° wide window for the cut to the west of Sondrestrom. (Most of the data for these times was taken looking through a pierce point to the west of Sondrestrom.) We have also shifted the scale of the percent occurrence so that zero occurrence lines up with a density of 5×10^5 cm^{-3}. This was done based on an estimate that predicts that this is the minimum density needed to produce 8an-dB fluctuation level. While both the simulations and the scintillations show a clear asymmetry about local midnight, the low densities after midnight suggest that at these times other sources of irregularities may be significant. This is the same type of conclusion as made by *Basu et al* [1995] for patches and scintillations around Thule.

Figure 4 shows similar results for March 1992. As before, the solid curve is the percent occurrence and the dotted curves are results from a number of simulations. Again, we see similar
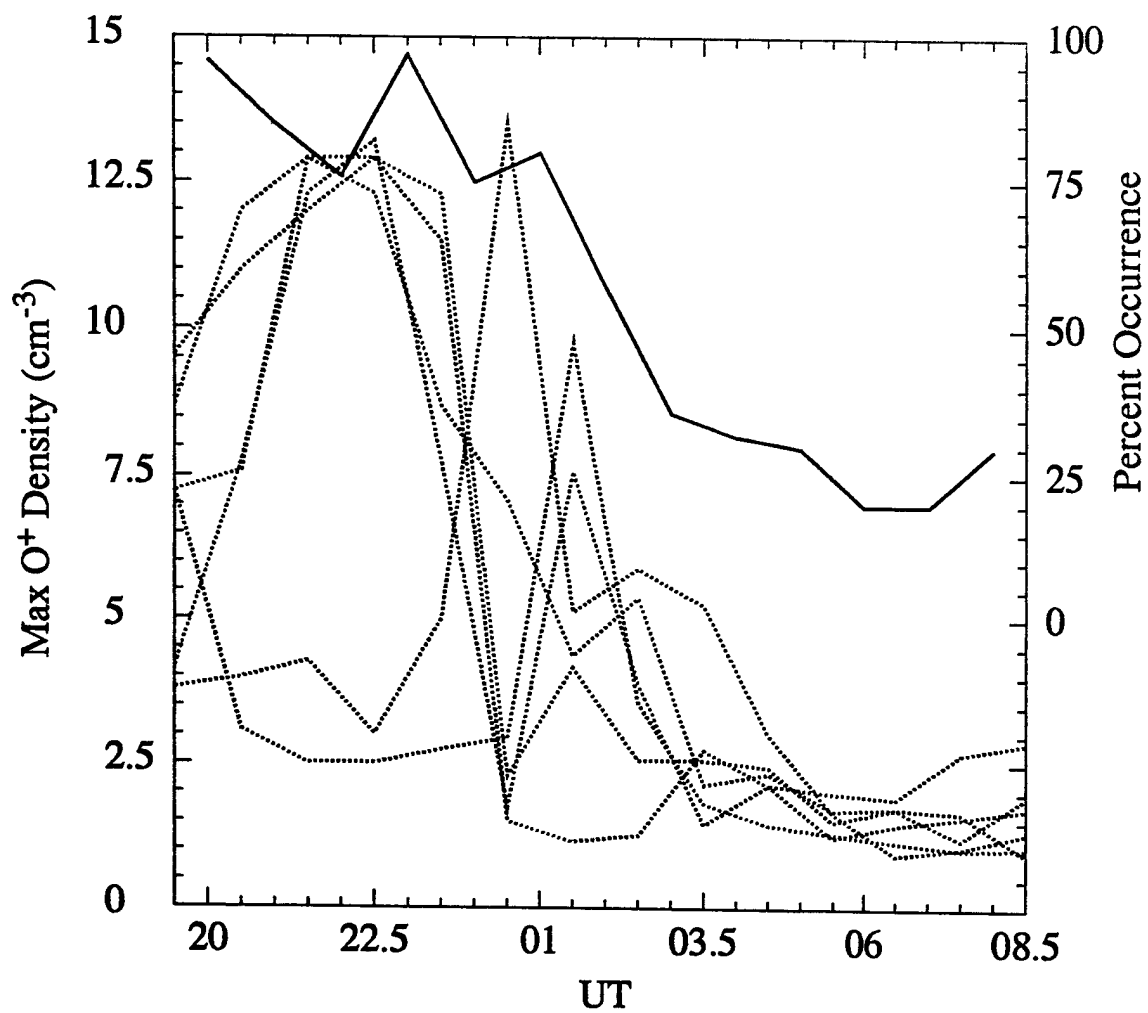
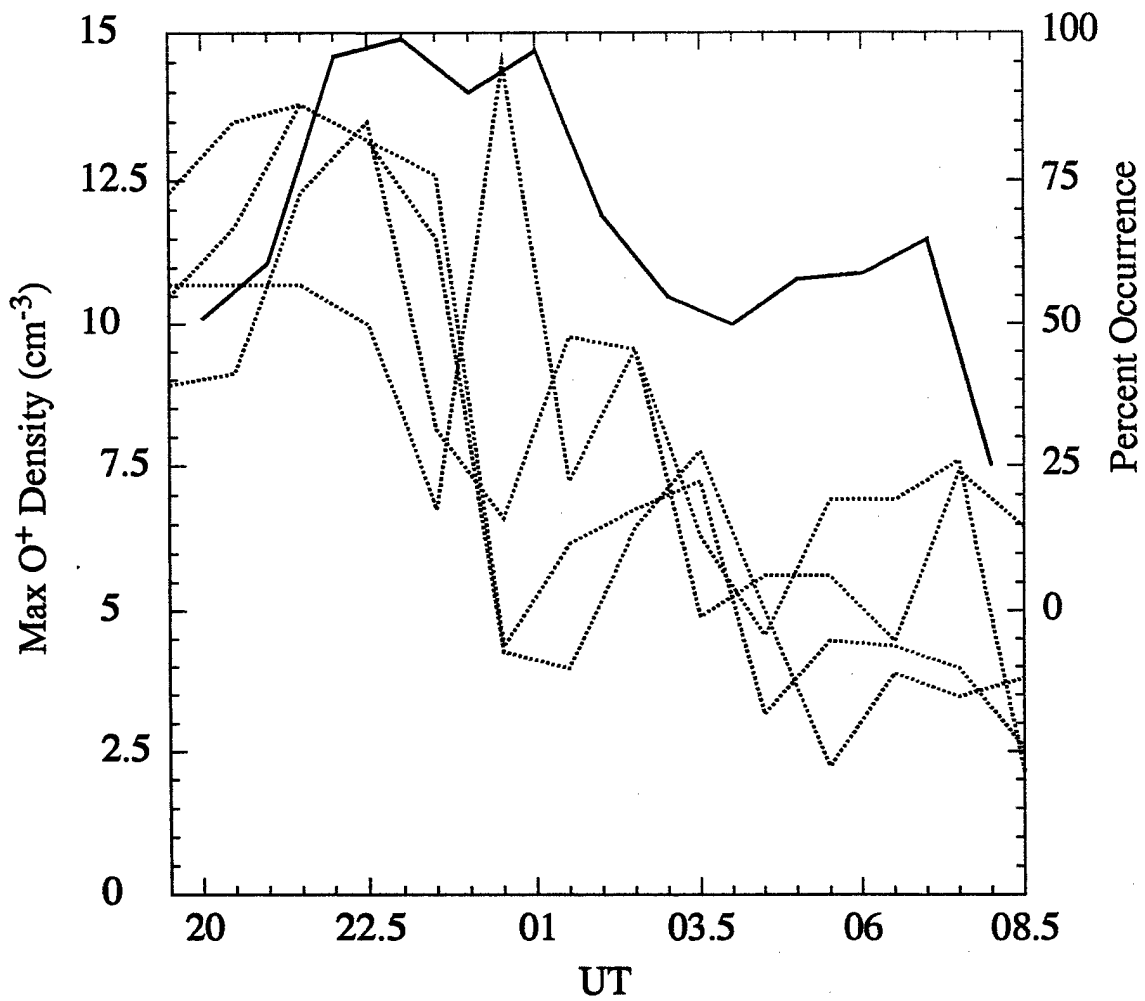**FIGURE 3.** December 1991 Scintillations (>8db) at 250 MHz

FIGURE 4. March 1992 Scintillations (>8db) at 250 MHz

behavior as a function of UT for both the scintillation observations and the simulations results. The asymmetry about local midnight (around the center of the plot) is not as marked as in December in both the simulations and the observations. Again in the post midnight sector the densities seem to drop lower than what is needed to explain all the scintillations.

Figure 5 is for June 1992. While the previous simulations were run for solar maximum conditions, by June 1992 the $F_{10.7}$ had fallen to 120. Thus, the June 1992 simulation used a moderate solar flux ($F_{10.7} = 120$, $F_{10.7a} = 136$). Here we see a much flatter distribution as a function of UT reflected in both the observations and simulation results. As in the other two months, there is a hint that at lower levels of scintillation activity the densities are lower than what is needed to explain > 8dB scintillations.

2.3. Effects of Time-Dependent Convection

A common theme of earlier work on modeling large-scale plasma structures has been to simulate the formation of these structures using solar produced plasma and the temporal and spatial structure in the E x B convection. In the last few years, a variety of new and more realistic sources for convection patterns have become available and it is critical that the Global Theoretical Ionosphere Model (GTIM) be capable of using them. In the past, each new convection source has required changes to GTIM that have made it increasingly complex and awkward to use. We have completed a major rewriting of the portion of GTIM that processes the convection patterns and calculates the E x B trajectories. A preprocessor has been written that constructs a convection database for the entire period being simulated. By shifting the handling of various convection sources to a preprocessor, we have made the source of the convection patterns transparent to GTIM and have facilitated their use.

The initial validation of this version of GTIM consisted of several parallel runs with the previous version and to date the new version has produced results consistent with the old version. The first study using a new source for convection has consisted of a simulation that used one hour of SuperDARN observations combined with Hairston/Heelis patterns. While this represented our first test of using SuperDARN convection observations, it also gave of us an opportunity to see how previous results would be affected when using more detailed convection patterns. The simulation considered a period when the IMF B_y made an abrupt switch from positive to negative followed an hour later by a switch back to positive. This type of B_y switching has been used in several studies of patches and blobs and so we were particularly interested in seeing the effect of using SuperDARN observations from such a period. Two simulations were performed. The first used three Hairston/Heelis patterns to approximate the switching of B_y. The second started with a Hairston/Heelis pattern, but then switched through a series of seven SuperDARN patterns (one every ten minutes) before ending back with a Hairston/Heelis pattern. To date we have compared the simulations at several high latitude locations. In Figure 6, we show N_mF_2 at Thule for Run 1 (solid curve) and Run 2 (dotted curve). We can see a dramatic dip in Run 2 that is caused by using the SuperDARN observations. However, a Run 1 and Run 2 for Sondrestrom show little difference. These initial results reinforce the idea that the sensitivity of the ionosphere to the convection pattern will depend not only on the details of the pattern, but also on where you are and when you are looking.
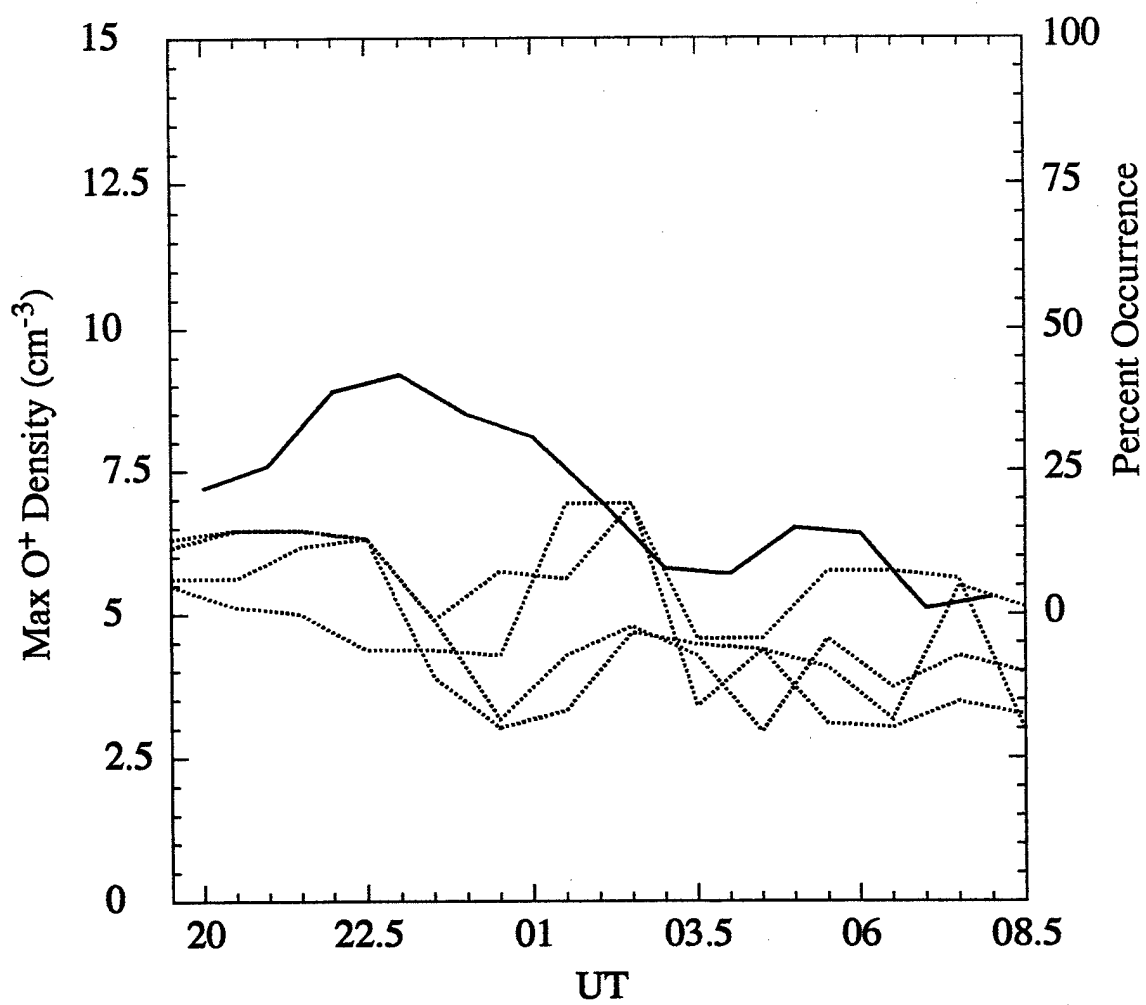
8

FIGURE 5. June 1992 Scintillations (>8db) at 250 MHz
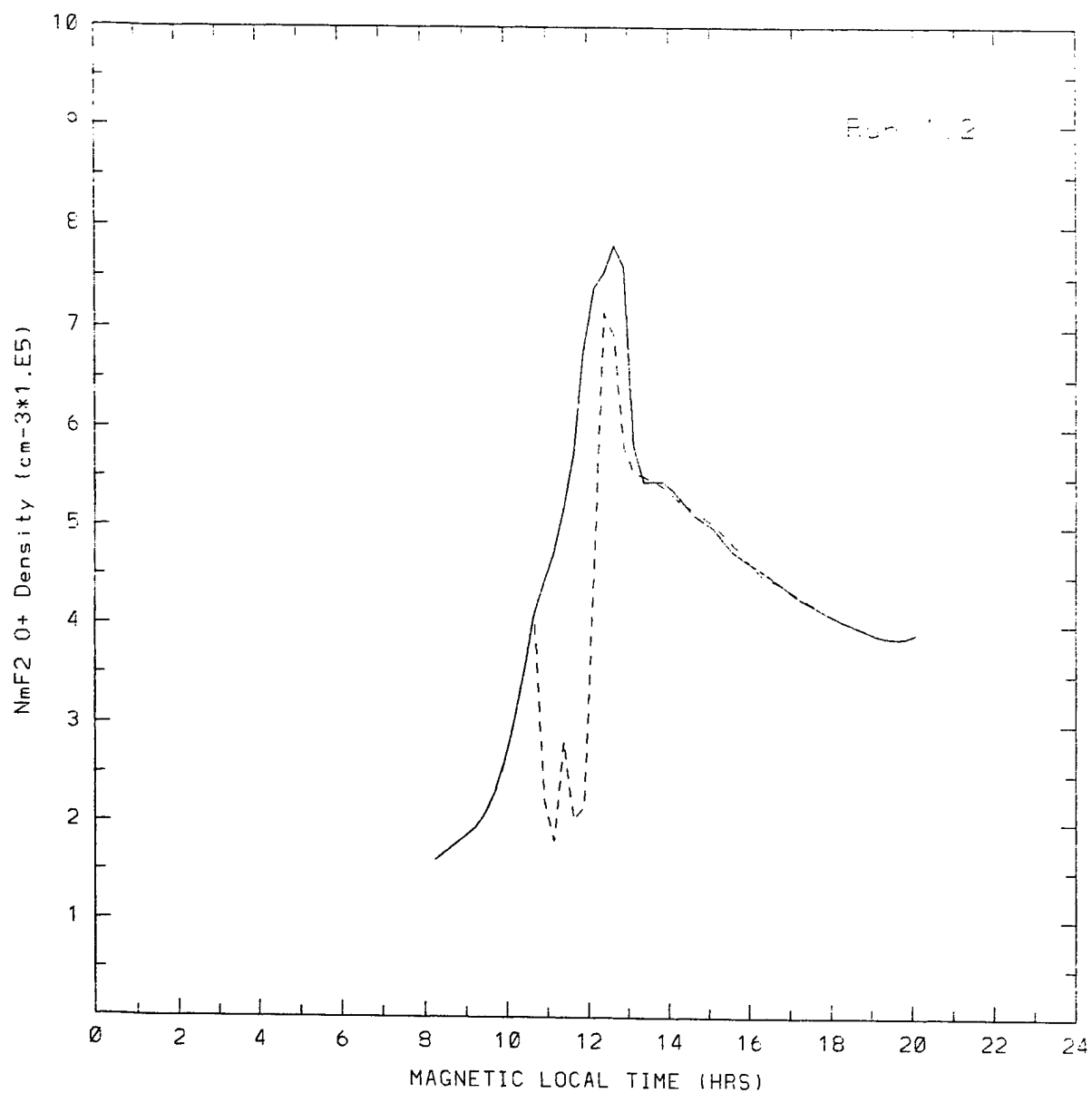
FIGURE 6. N_mF2 at Thule Run 1(Solid Curve) Run 2(Dotted Curve)

We have also examined several nighttime auroral locations and find that the simulation using SuperDARN observations produced blob-like structures much like our earlier simulations. The point here is that this gives us increased confidence in our previous blob simulations that have used simple time variations to describe the behavior of the convection pattern.

A preprocessor has been written that constructs a convection database using the Weimer convection model and a series of runs have been performed comparing the effects of using different sources for the convection. In Figure 7, we show N_mF_2 every 15 minutes at 85(N), 85(E). The solid curve is a simulation that used a single Hairston-Heelis pattern and the dotted curve is a run using three Hairston-Heelis patterns chosen to approximate a switching of B_y. Figure 8 again shows the three Hairston-Heelis simulation (dotted curve) along with a simulation that used one hour of 10-minute resolution SuperDARN data (solid curve). In Figure 9, we show the SuperDARN simulation (solid curve) and a simulation that used one hour of 10-minute resolution Weimer convection (dotted curve). What we see is another example of the ionosphere's sensitivity to the details of the convection pattern.

Another simulation was performed that used 24 hours of IMF to construct 24 hours of Weimer convection. This was compared to a simulation that used SuperDARN for 5.5 hours of that 24 hours and Weimer for the remaining time. Figure 10 shows the N_mF_2 for the Weimer run (solid curve) and the SuperDARN/Weimer run (dotted curve). The results diverge after 13.5 MLT (around 16 UT when SuperDARN convection begins) and continue diverging until near the end. They come back together as both simulations go back to using the same convection patterns. Again, we see that the model results are sensitive to the convection used even when the two sources of convection are supposed to be representing the same period.

However, the IMF data and SuperDARN data came from 10 January 1996 which is from a solar minimum period. We have repeated the previous simulations, but now specifically for 10 January 1996. That is, we have used the geophysical parameters specific to that day. We also have the digisonde data from Qaanaaq for that day. This means we could make a day specific simulation and compare it with observations also specific to the particular day.

As we see in Figure 11, we find that both the Weimer (short dashes) and SuperDARN/Weimer (long dashes) calculations produce a more realistic ionosphere over Qaanaaq. They show structure that is qualitatively the same as what is seen (solid curve). A steady-state convection simulation does not. Also, the Weimer and SuperDARN/Weimer calculations give tantalizing hints of quantitative agreement with some of the observed ionospheric structures. At the same time, the differences between the Weimer simulations and the SuperDARN/Weimer simulations suggest that getting fairly precise agreement with observed structure might require fairly detailed knowledge of the convection pattern. What is clear is that much work is needed to develop a quantitative understanding of the ionosphere's sensitivity to time varying convection.
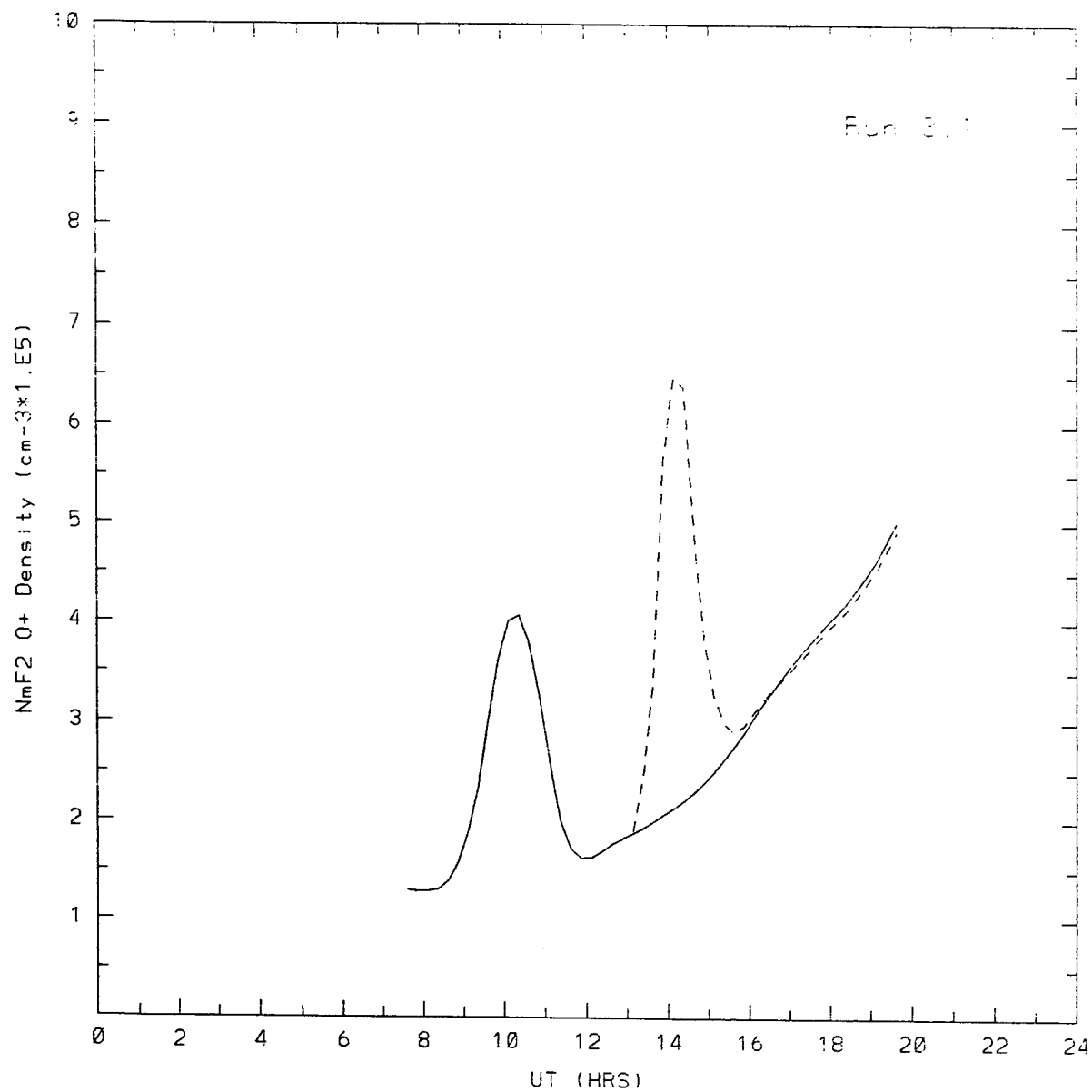
FIGURE 7. N$_m$F2 Every 15 Minutes At 85(N), 85(E) Hairston-Heelis Simulations
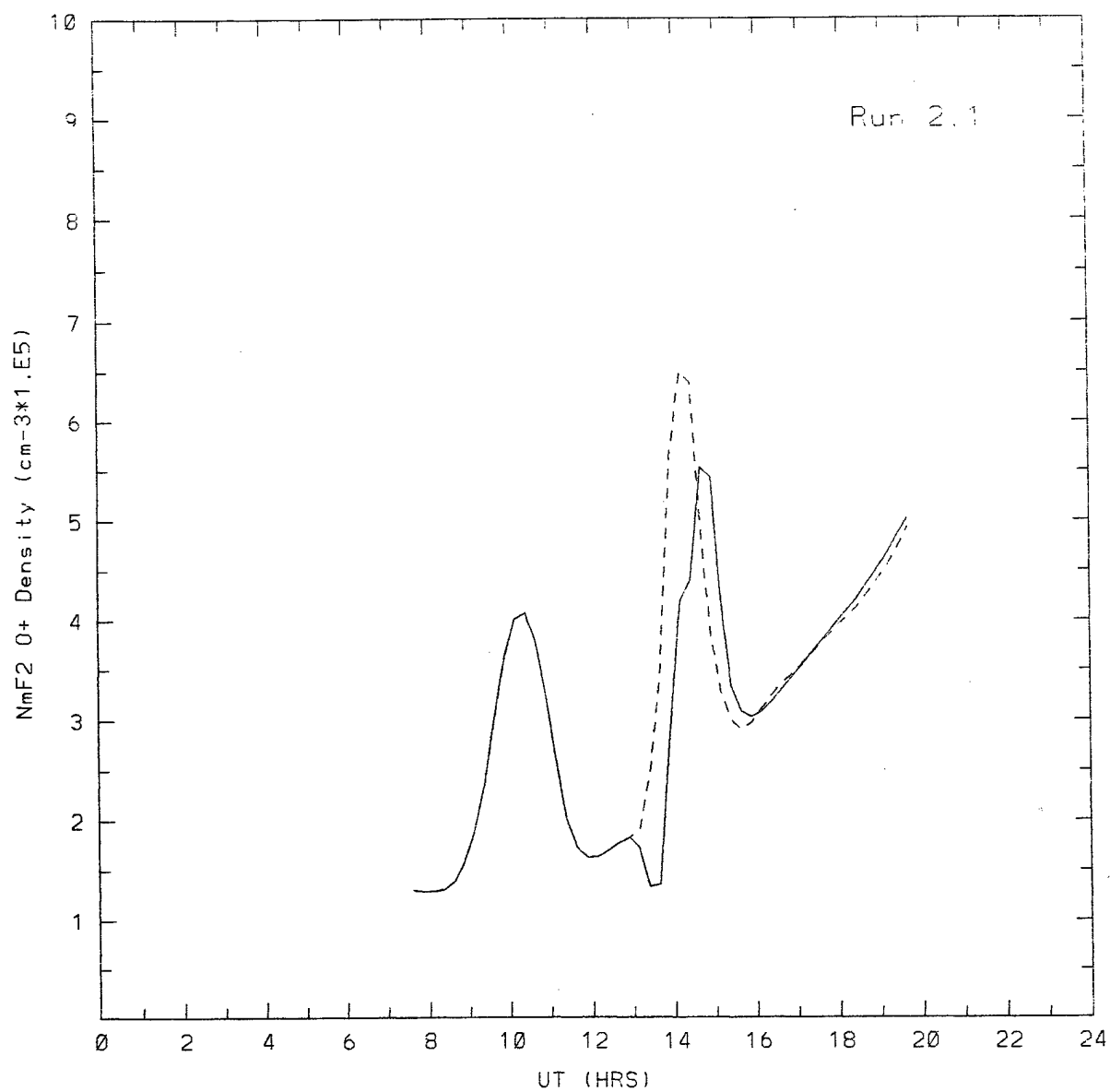
FIGURE 8. N_mF2 Every 15 Minutes At 85(N), 85(E) Hairston-Heelis Simulation And SuperDARN Data
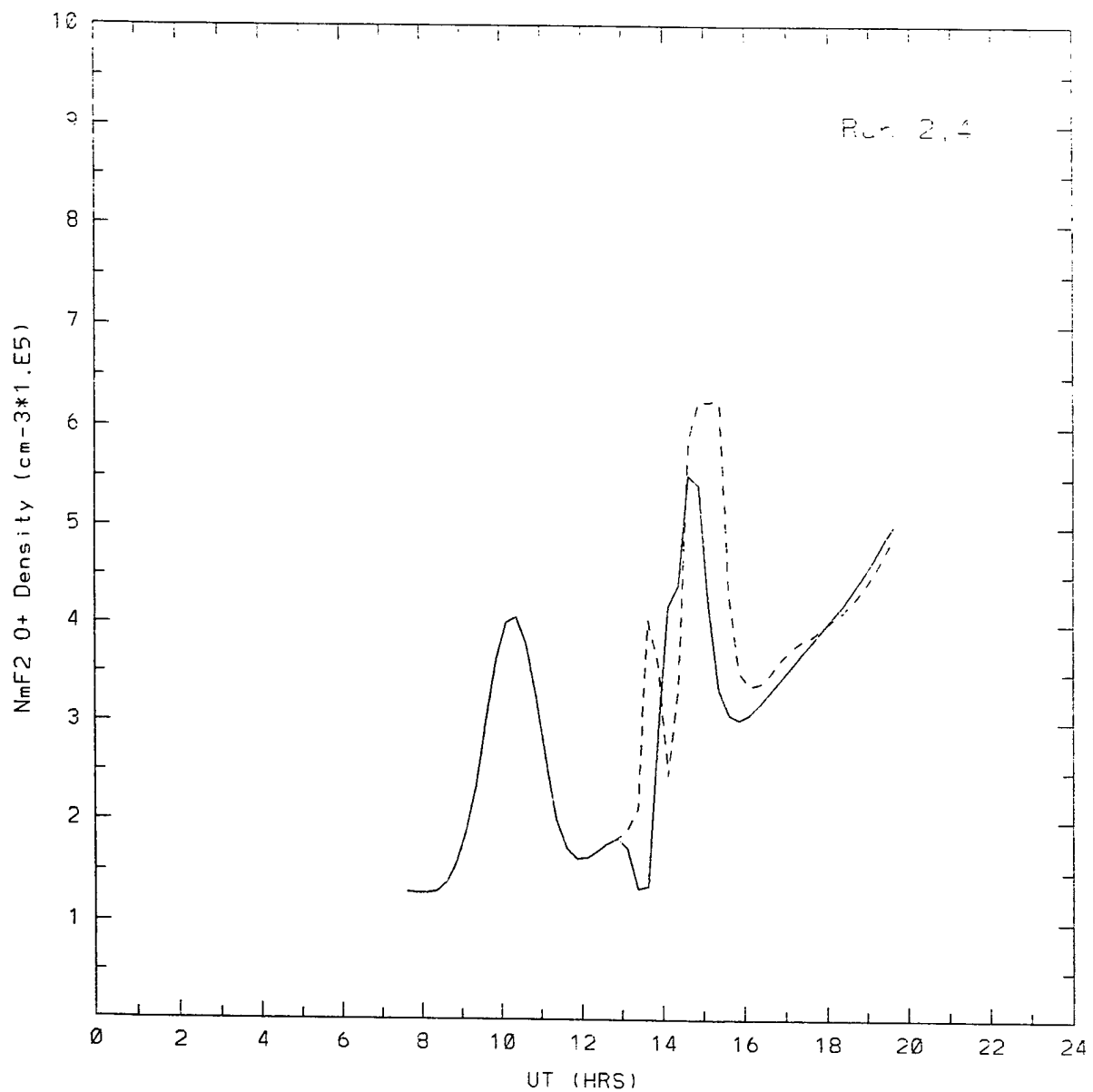
FIGURE 9. N_mF2 Every 15 Minutes At 85(N), 85(E) SuperDarn Data And Weimer Convection

Thule   15 min

HW, HWMW

NmF2 O+ Density (cm-3*1.E5)

MAGNETIC LOCAL TIME (HRS)
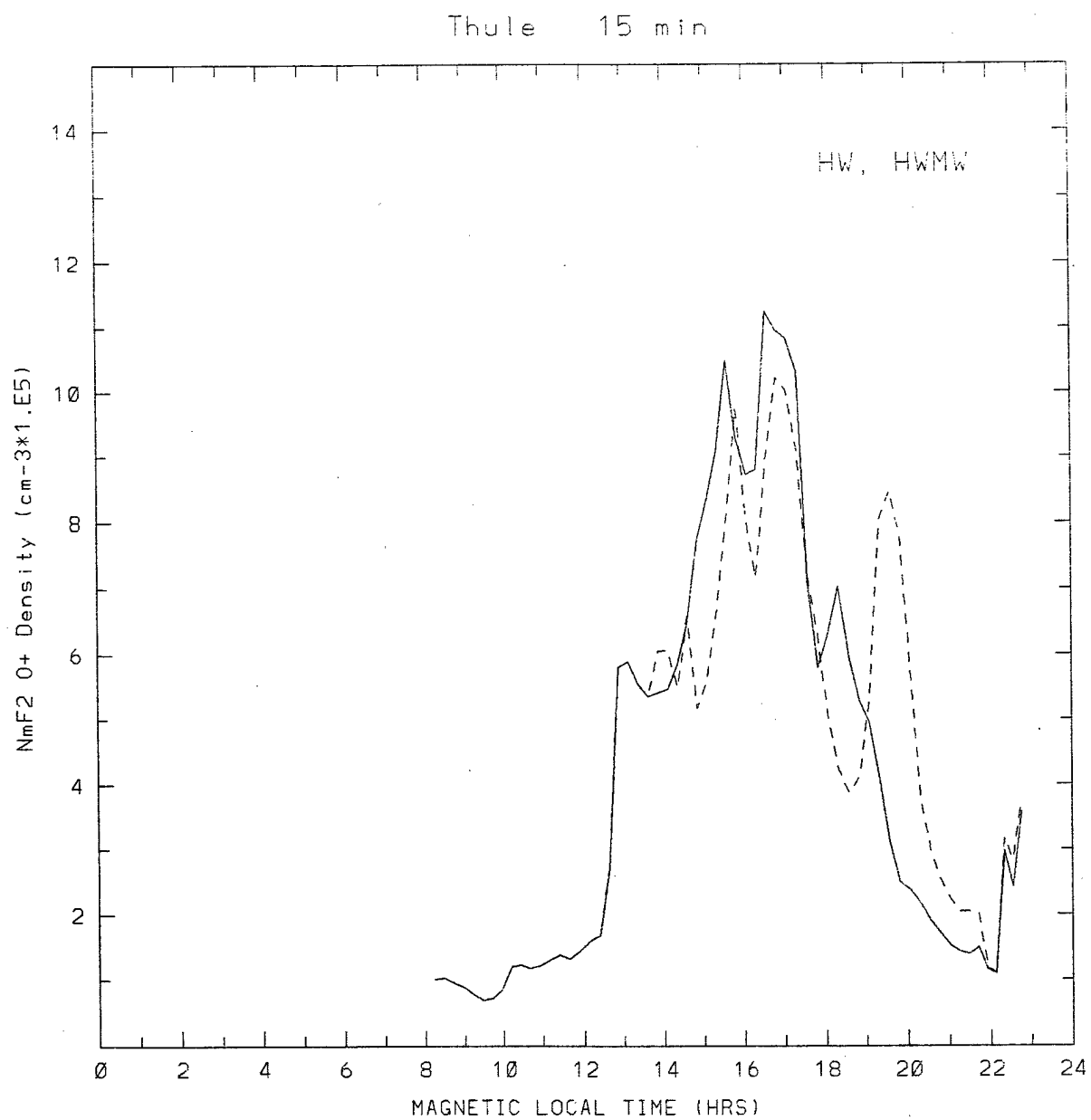
FIGURE 10. N_mF2 For Weimer Run (Solid Curve) And SuperDARN/Weimer Run (Dotted Curve)
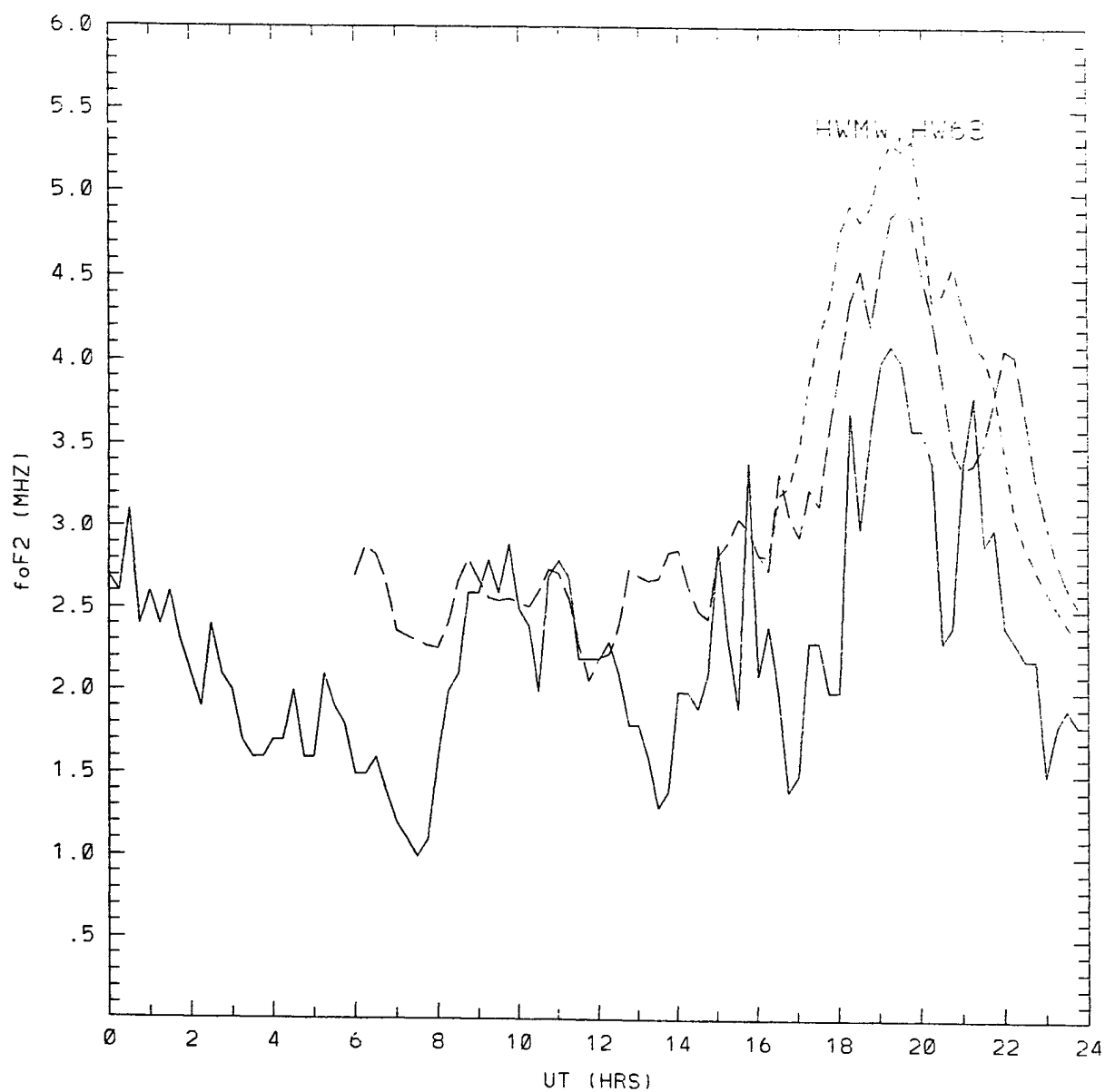
FIGURE 11. foF2 Values For Weimer And SuperDARN/Weimer Calculations Over Qaanaaq Jan. 10, 1996

2.4. GPS Occultation Studies

Validation of Ionospheric Inversion Algorithms with NPOESS/GPSOS Type Sensor

In previous work we have simulated GPSMET observations and performed various inversions on those simulated observations. We have also demonstrated that our software can produce "reasonable" looking results using actual GPSMET data. The next step has been to perform actual validations using coincident GPSMET and digisonde observations.

The validation process consists of examining the GPSMET occultation ephemeris for a given period and identifying coincidences with ground-based digisondes. Once candidate cases are identified we check to see if GPSMET data are available and if processed digisonde observations are also available. If the data is available, then when received we perform the inversion of the occultation data and compare with true height profiles derived from the digisonde observations. Here, we begin with a description of our first attempts to validate our Abel inversion algorithm, matrix inversion algorithm, and the results of previous simulations using data from a period in February 1997.

In Figure 12, we show a daytime low latitude example of a coincidence between an occultation and the digisonde observation at Cachoeira Paulista, Brazil. The occultation is from day 51, 1997 and occurred from 1324 to 1332 UT (1013 to 1021 LT). The occultation was centered on a location that was 2° north and west of the digisonde location. The solid curves are true height profiles derived from the digisonde observations taken at 1315 and 1415 UT. The curve of long dashes is a PIM profile for the time and location of the occultation. The curve of short dashes is the result of an Abel inversion being applied to the GPSMET data. The curve of dots is the result of the matrix inversion algorithm being applied to the GPSMET data with the assumption of a PIM horizontal behavior. From around 300 to 150 km, we see good agreement between the inversions and the observed profile. The F_2 peak density and height are underestimated, but the inversions clearly give a better estimate than that provided by PIM.

Another daytime example is given in Figure 13 for a coincidence between an occultation and digisonde observations from Ramey, Puerto Rico. The occultation is from day 34, 1997 and occurred from 1952 to 1959 UT (1507 to 1520 LT). The occultation center was 3° north and west of the digisonde. The solid curves are true height profiles derived from the digisonde observations taken at 1930 and 2000 UT. The curve of long dashes is a PIM profile at the center of the occultation and the curve of short dashes is the results of the Abel inversion. The curve of dots is the result of the matrix inversion algorithm being applied with the assumption of a PIM horizontal behavior. We see good agreement through much of the lower F region. In this case the Abel performs better than the matrix inversion using PIM horizontal behavior and both algorithms produce a better bottomside shape than does PIM. The inferred profiles are not as smooth as the previous case because only low rate (.1 Hz) occultation data was available on day 34 as compared to medium rate (1 Hz) data on day 51.

In Figure 14, we show another example from a coincidence near Cachoeira Paulista that occurred on day 40, 1997. This nighttime occultation was at 0432 to 0440 UT (0153 to 0201 LT) and around 6° north and east of the digisonde. The solid curves are true height profiles derived from
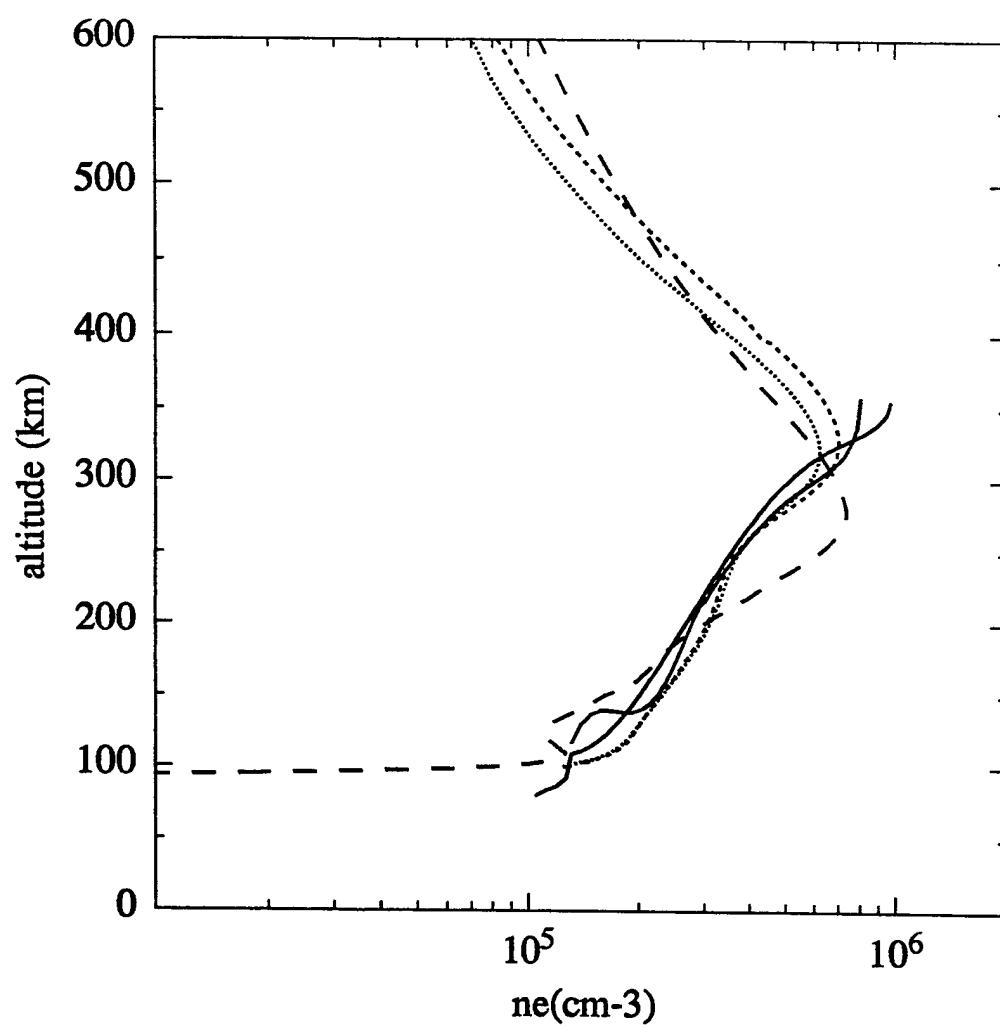
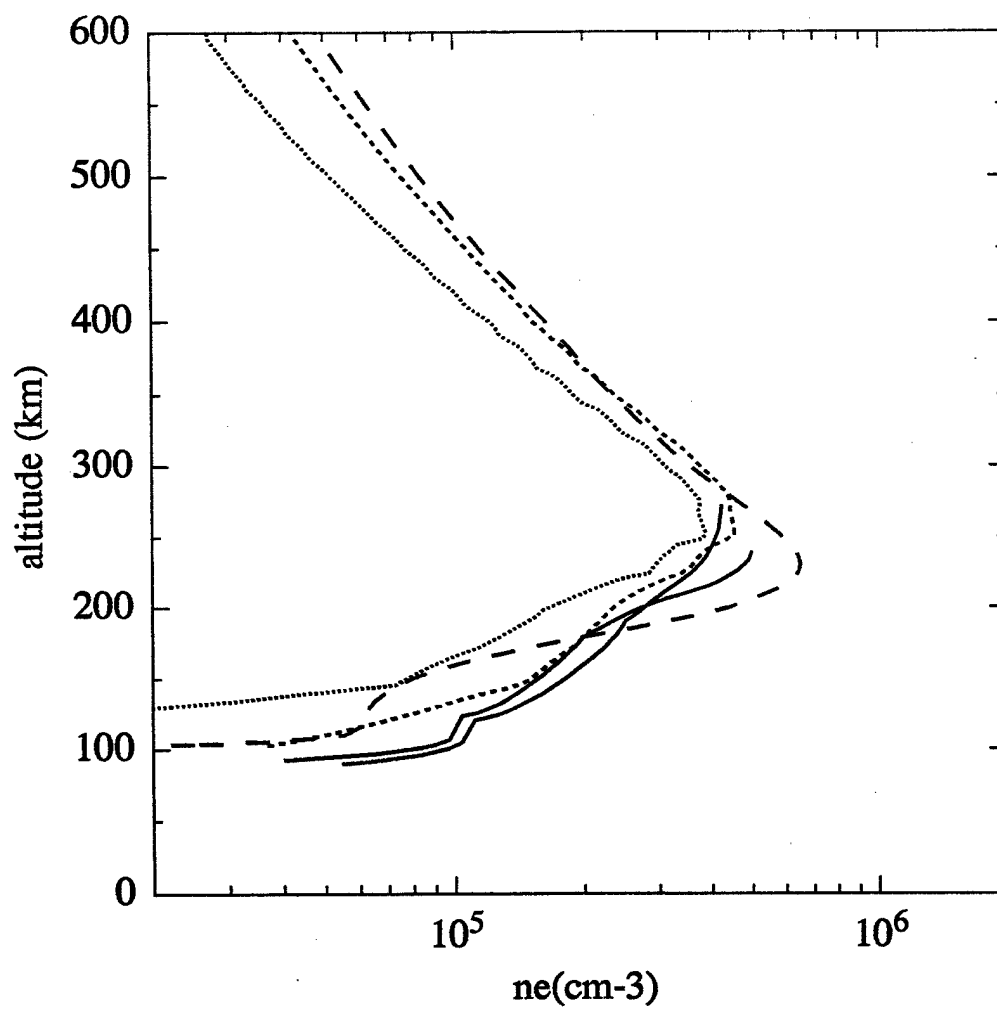**FIGURE 12.** Digisonde, PIM, Abel, & LU(PIM) Day 51

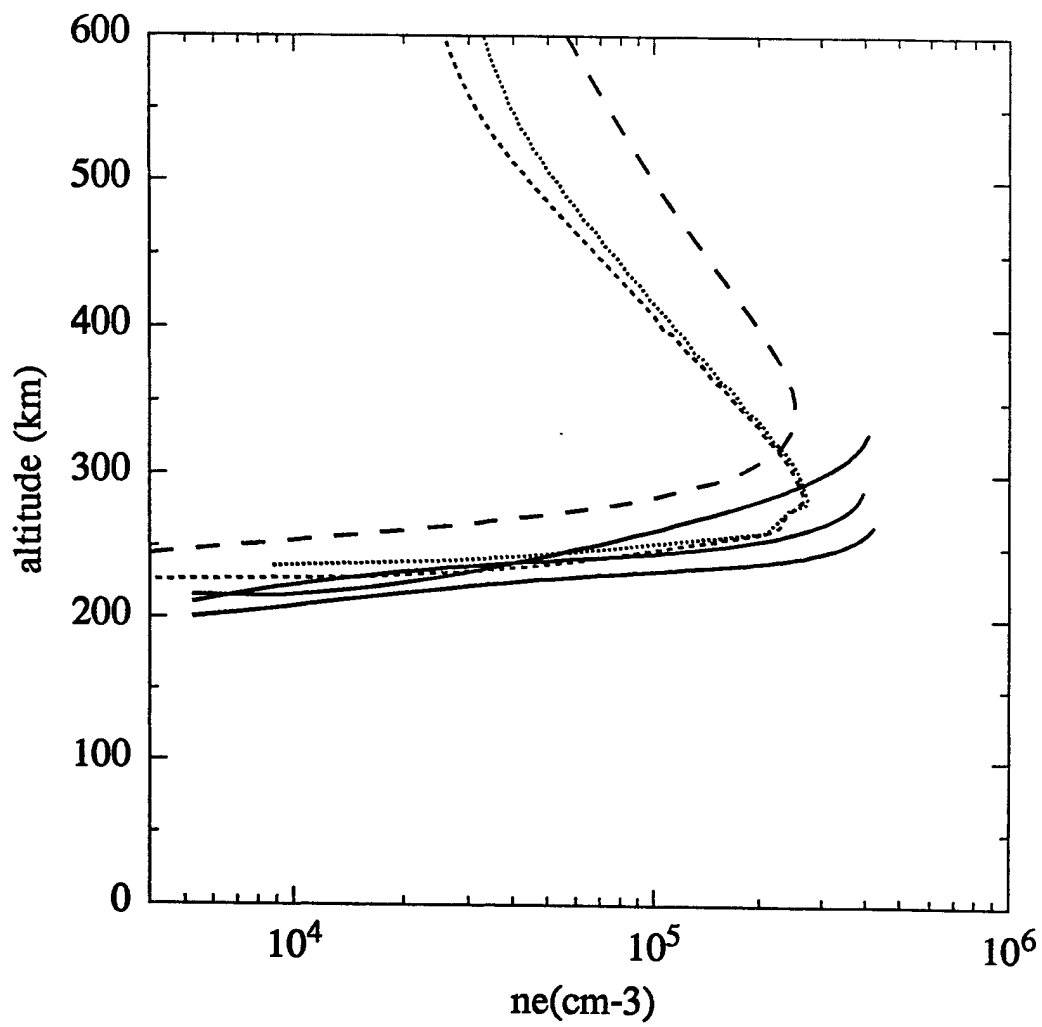**FIGURE 13.** Digisonde, PIM, Abel, & LU(PIM) Day 34

19

FIGURE 14. Digisonde, PIM, Abel, & LU(PIM)   Day 40

20

the digisonde observations taken at 0415, 0430, and 0445 UT. Again, the curve of long dashes is a PIM profile for the time and location of the occultation. The curve of short dashes is the result of an Abel inversion being applied to the GPSMET data. The curve of dots is the result of the matrix inversion algorithm being applied to the GPSMET data with the assumption of a PIM horizontal behavior. We see a good match between h_mF_2 given by the inversions and that observed at 0430 UT. The location of the bottom of the F layer matches well, but we see that that N_mF_2 from the inversions is underestimated. Again, we see that the inversions do a better job than PIM in predicting the bottomside of the F region.

Next we completed three other nighttime cases and found that two of them show similar results to the nighttime example given above. The one exception involved a coincidence near Jicamarca, Peru. In that case, a PIM profile did significantly better than the inversions. However, the occultation was over 11° south of Jicamarca and it is very possible that the differences between the inversions and the Jicamarca digisonde observations could be the result of spatial variations in that day's ionosphere. Excluding this one day, we can say that a consistent feature of all the cases is that inversions of GPSMET more accurately predict the bottomside F region than the climatological model PIM. Also, the agreement is qualitatively comparable to our earlier simulation results. However, a more quantitative assessment of the simulation results will require many more validation cases. Also, this effort has focused on using range delay or carrier advance to infer the EDP, however the ionosphere also causes a bending of the radio waves and this effect can also be used to infer the EDP (*Hoeg et al.*, 1995; *Hajj and Romans*, 1996). Thus a validation effort using this method should eventually be pursued in parallel with our current effort.

Continuing work from this period, we have now examined seven daytime and eight nighttime cases all in the American or Brazilian sector. The northern hemisphere cases are all daytime and range in geographic latitude from 21.8° to 34.7°. All the southern hemisphere cases are around Cachoeira Paulista (-23.29(N), -45.8(E)), Brazil except for the one nighttime case that is in the vicinity of Jicamarca, Peru. The six daytime cases in the northern hemisphere are all in the early afternoon (~ 1237-1520). The one daytime southern hemisphere case was in the late morning at around 1017 LT. All the nighttime cases are in the southern hemisphere and occur in the early morning (~ 0015-0314 LT).

The daytime F_2 peak results are summarized in the following table.

| | Avg. Digisonde | | PIM | | PIM | | ABEL | | ABEL | |
Day	N_mF_2	h_mF_2	N_mF_2	frac	h_mF_2	del h	N_mF_2	frac	h_mF_2	del h
34	4.60	256	6.99	1.52	234.5	-21.4	4.55	0.99	253.9	-2.05
36	5.65	255	5.84	1.03	234.0	-20.6	5.29	0.94	271.0	+16.4
40	6.25	263	5.13	0.82	250.0	-12.5	6.12	0.98	269.0	+6.5
42	5.15	270	5.28	1.03	238.0	-31.6	6.10	1.18	262.0	-7.6
45	3.88	229	4.90	1.26	222.0	-7.0	4.10	1.06	246.0	+17.0
47	5.50	258	5.40	0.98	228.5	-29.0	4.80	0.87	265.0	+7.5
51	8.89	358	7.35	0.83	279.5	-78.2	7.00	0.79	327.5	-30.2

N_mF_2 is the maximum of the F_2 peak in units of 10^5 cm^{-3} and h_mF_2 is the height of the F_2 peak in kilometers. The quantity frac is the ratio of either the PIM or ABEL N_mF_2 to the averaged observed N_mF_2. The quantity del h is the PIM or ABEL h_mF_2 minus the averaged h_mF_2 inferred from the digisonde observations. The average of the digisonde observations is simply the average of the two observations that bracket the center time of the occultation. We can see that the Abel is generally within 20 percent of the observed N_mF_2 and within 20 km of the observed h_mF_2. Abel does better than PIM (six out of seven times) in predicting h_mF_2 while PIM performs a bit better for N_mF_2 (four out of seven). Though the worst case for Abel's N_mF_2 (.79) is better than the PIM's worst case (1.52). Also, while day 51 has the poorest F_2 peak coming from the Abel inversion, an examination of the entire bottomside profile showed that it had the best bottomside fit out of all the daytime cases. This illustrates how focusing on only the F_2 peak as a measure of accuracy can be misleading when assessing the quality of the inversion.

In the seven nighttime cases near Cachoeira Paulista, the Abel did a better job estimating the altitude of the layer (5 times) than did PIM. However, Abel generally underestimated N_mF_2. There were also two cases where Abel predicted nonexistent enhanced E-regions. A source of uncertainty is that the coincidences were not as close as you would like and thus the results are sensitive to whatever spatial and temporal variability existed on the given day.

There has been a digisonde operating at Jicamarca, Peru for the last several years that provides us with a good opportunity for performing more validation at low latitudes. We searched the GPSMET database for coincidences with Jicamarca, Peru and found 12 cases. These 12 cases were all setting occultations. We have not yet searched for the rising cases. We have again performed two types of inversions: (1) Abel inversions and (2) matrix equation solution (MES) inversions (assuming a PIM horizontal behavior). Four of the cases had anti-spoofing off and have well behaved phase data. The other days had anti-spoofing on and showed rather strange behavior. The behavior was strange in that it was unexpected and unlike anything we have seen previously in ground-based GPS data. What were seen in some cases were drop outs of phase observations followed by some sort of recovery. Other cases had the phase simply flatten out leading to inverted profiles that looked as if they had their F_2 peak cut off. All this behavior was correlated with large decreases in the signal to noise for L2. Attempts to use the L1 phase and group measurements produced profiles with severe discontinuities. At this point, it is unknown if these types of problems are wide spread in the anti-spoofing on cases.

For the four anti-spoofing off cases, we have compared to digisonde profiles and the agreement is very mixed. In one case, the N_mF_2s agree well, h_mF_2s are 15 km apart, but the inversions' bottomsides are around 50 km too high. Another case gives excellent agreement at the F_2 peak and all through the F_1 region. The third case produces a well-behaved daytime profile but the entire profile is around 30% below the digisonde observations. Finally, the fourth case produced an odd shaped F_2 peak that severely underestimates N_mF_2. We are continuing to analyze all these cases, but we can say that this behavior is qualitatively similar to our simulation results that likewise showed a mixture of results at low latitudes.

Simulations of GPS Occultations

Work has continued on using the matrix equation solution (MES) approach to explore the use of other measurements to help constrain the inversion process. In earlier work, we examined the use of in-situ electron density measurements to constrain the inversion. Here, we are examining the usefulness of having N_mF_2 as might be obtained at night from a photometer onboard the same satellite as the GPS receiver. We performed a series of simulations in order to compare different approaches for constraining the inversions. We considered some nighttime cases (3 solar min and 3 solar max) that we had previously found to cause problems for the Abel inversion. We ran four different inversion algorithms. The first used just the in-situ measurement to specify the horizontal structure at all altitudes. The second linearly interpolated from the behavior of the in-situ measurement at the satellite altitude to an isotropic behavior at the h_mF_2 determined by an Abel inversion. The third uses the horizontal behavior of N_mF_2 in a layer about the h_mF_2 determined by an Abel inversion. The fourth interpolates from the in-situ behavior at the top to the behavior of N_mF_2 at the h_mF_2 determined by an Abel inversion. We found that none of the methods improved our ability to retrieve the nighttime E region. While the fourth method generally produced the best results, the improvements were modest and in one case h_mF_2 was still 15 km too high.

FY 1998 Weather Products Test Bed (WPTB) Observational Scenes

As part of our work on GPS occultations, we are providing observational scenes from coincidences between ground-based digisonde observations and GPS/MET occultations. The scenes consist of GPS/MET data and digisonde data. We have created a subdirectory in the anonymous ftp directory on andersun (pub/decker/GPSMET_data) and have placed GPS/MET data there. There are data from five days in February 1997. They include nine occultations that are coincident to some degree with ground-based digisonde observations. There are five daytime cases and four nighttime cases and they are all in the American or Brazilian sector. The northern hemisphere cases range in latitude from 21.8° to 34.7° geographic. All the southern hemisphere cases are from around Cachoeira Paulista {-23.29°(N), -45.8°(E)}. The four daytime cases in the northern hemisphere are all in the early afternoon (approximately 1300-1500 LT). The one daytime southern hemisphere case was in the late morning at around 1017 LT. All the nighttime cases are in the early morning (approximately 0100-0300 LT).

There are three types of files included: GPSMET RINEX data file (level 1), GPS POD (Precise Orbital Determination) file (level 2), and LEO (Low Earth Orbiting) POD file (level 2). The RINEX file is the standard format for GPS data files (except these have signal-to-noise added to the file) and the POD files have the ephemeris for the GPS satellites and the GPS/MET LEO satellite.

2.5. Ionospheric Modeling Using Systems of Plasma Kinetic Equations

Work has continued on developing a numerical solution to a kinetic equation for the ion distribution function. Preliminary runs of the code were giving solutions that were not consistent with the moment equations derived from the kinetic equation, that is, the conservation laws were not being satisfied. This came about because particles were being lost out the bottom of our grid. While some of this was caused by a lack of grid points, it proved crucial that the ambipolar field

used in the initial calculation should not be too crude an approximation. Once an improved initial ambipolar field was chosen, the kinetic equation could be iterated with a set of 8 moment equations to give a self-consistent solution for the distribution function and the ambipolar field. Solutions thus obtained now satisfy the required conservation laws.

As further logic was developed to see how well the conservation equations for the moments of the distribution function could be satisfied, a contour subroutine was having difficulties. The difficulties came from using unrealistic input parameters in the calculation. When inputs that were physically reasonable were used, the problems disappeared. A series of calculations have been made using appropriate inputs and the results closely resemble experimental results.

Work began on writing software that finds the solution to the ion kinetic equation for ions moving in the negative direction. Inconsistencies were found in the initial formulation of the differential equation being used. A guess was made as to the probable form of the equation and this form was programmed. While there may be some changes to the logic if the guess is incorrect, the majority of the software involves handling the extended grid needed for treating negative velocities and is independent of the precise form of the differential equation. Thus any adjustments needed when the form of the differential equation is clarified should be relatively minor.

2.6. GPS Accuracy Issues

A request has been made by the ACC/Army to AFSPC/DORW and 55 SWX to provide a tailored navigation product that will give near real-time information on the magnitude of the navigation/location errors that the PLGR GPS receiver will experience due to uncorrected ionospheric effects. We have been performing some of the necessary research that is required for developing this tailored product.

The ionosphere is the most highly variable source of error to GPS navigation and positioning. GPS users with access to both the L1 and L2 frequency signals automatically correct for the highly variable ionospheric contribution to range error by computing the difference in the time delays between the two operating frequencies. GPS users who are limited to the L1 frequency must use an alternate method to correct for the ionospheric effect. For these single frequency users, an Ionospheric Correction Algorithm (ICA) was designed in the mid-1970's to provide a correction for the ionospheric range error. The algorithm consists of eight coefficients transmitted as part of the GPS satellite navigation message to the user. These coefficients were designed to represent global behavior of the ionospheric contribution to range error with an approximate 50 percent accuracy in the mid-latitudes. Studies have tested the performance of the ICA and have verified that it meets or exceeds the required 50 percent accuracy requirement.

The U.S. Department of Defense (DoD) has obtained over 100,000 Precision Lightweight GPS Receivers (PLGR) from Rockwell's Collins Avionics and Communications Division (CACD). PLGR is designed for handheld and land-mobile operations and can be installed in a variety of military vehicles. It is a single-frequency system and provides the Precise Positioning Service (PPS) intended solely for military and select government users. Its low-power consumption makes it ideal for portable operations by infantry and special operations troops. These receivers are now in daily use by the U.S. and allied troops around the world, providing position location

and timing data to enhance mission synchronization and operating efficiencies. Since the PLGR is a single frequency system, its largest remaining source of error is the ionosphere. Thus, the goal of this work is to develop the ability to identify, in near real-time, the potential errors in position that the PLGR would experience due to uncorrected ionospheric errors.

The important parameter responsible for ionospheric time delay is the total number of electrons encountered by the radio wave on its path from each satellite to the GPS system user. This total electron content (TEC) is a function of many variables, including long-and short-term changes in solar ionizing flux, magnetic activity, season, time of day, user location, and viewing direction. TEC is directly proportional to the time delay encountered by the single frequency GPS user.

Our first step was to examine the magnitude of ionospheric error that can be introduced to a single-frequency receiver using the current GPS Single-Frequency Algorithm (SFA). Figure 15 illustrates some of these results by comparing contour plots of worldwide ionospheric TEC based on calculations of the theoretical Parameterized Ionospheric Model (PIM) with contours of TEC based on the current SFA. This figure is based on calculations for a solar maximum, equinox period at approximately 20 hours universal time. Note that the PIM and SFA contours show a generalized agreement in the mid-latitudes, but that the SFA fails to model the highly variable equatorial anomaly region. This then suggests that in the mid-latitudes, single-frequency GPS users would make a reasonable correction for the ionosphere under average ionospheric conditions. In the low latitude region, however, single-frequency GPS users would potentially underestimate the ionosphere by as much as 100 percent at local noon.

The next step was to examine the magnitude of the differences between ionospheric measurements made using a dual-frequency system with those generated with the SFA. The dual-frequency data used in this study was recorded at Ascension Island during the month of April 1997. Ascension Island is located at −7.9° latitude and −14.41° longitude. This site's geomagnetic latitude is at approximately −19°, very near the equatorial anomaly region. For comparison with the dual frequency measurements, we used the single-frequency GPS user algorithm to compute the ionospheric correction available to single frequency users along the same lines of sight from Ascension Island. In Figure 16, we have plotted the equivalent vertical TEC versus sub-ionospheric local time for nine consecutive days in April 1997. The solid curves represent the dual-frequency measurements along different lines-of-sight and the long dashed curves represent the single frequency model calculations along the same lines of sight. The differences seen in the dual-frequency TECs at common local times is primarily the result of the measurements recorded along different lines of sight from one receiver location. Note that these differences along with the large day-to-day variability of the dual-frequency measurements are not captured by the model calculations. Much of the day-to-day variability seen at Ascension Island is due to the site's close proximity to the equatorial anomaly region. Recall that the largest values of TEC and the largest ionospheric gradients over latitude are observed in this region. Figure 16 illustrates that the single-frequency correction was largely deficient during the daytime hours and did not capture the large day-to-day variability of the dual-frequency TEC measurements at this low latitude location.

Parameterized Ionospheric Model (PIM)

Single Frequency Algorithm (SFA)

Difference (PIM − SFA)
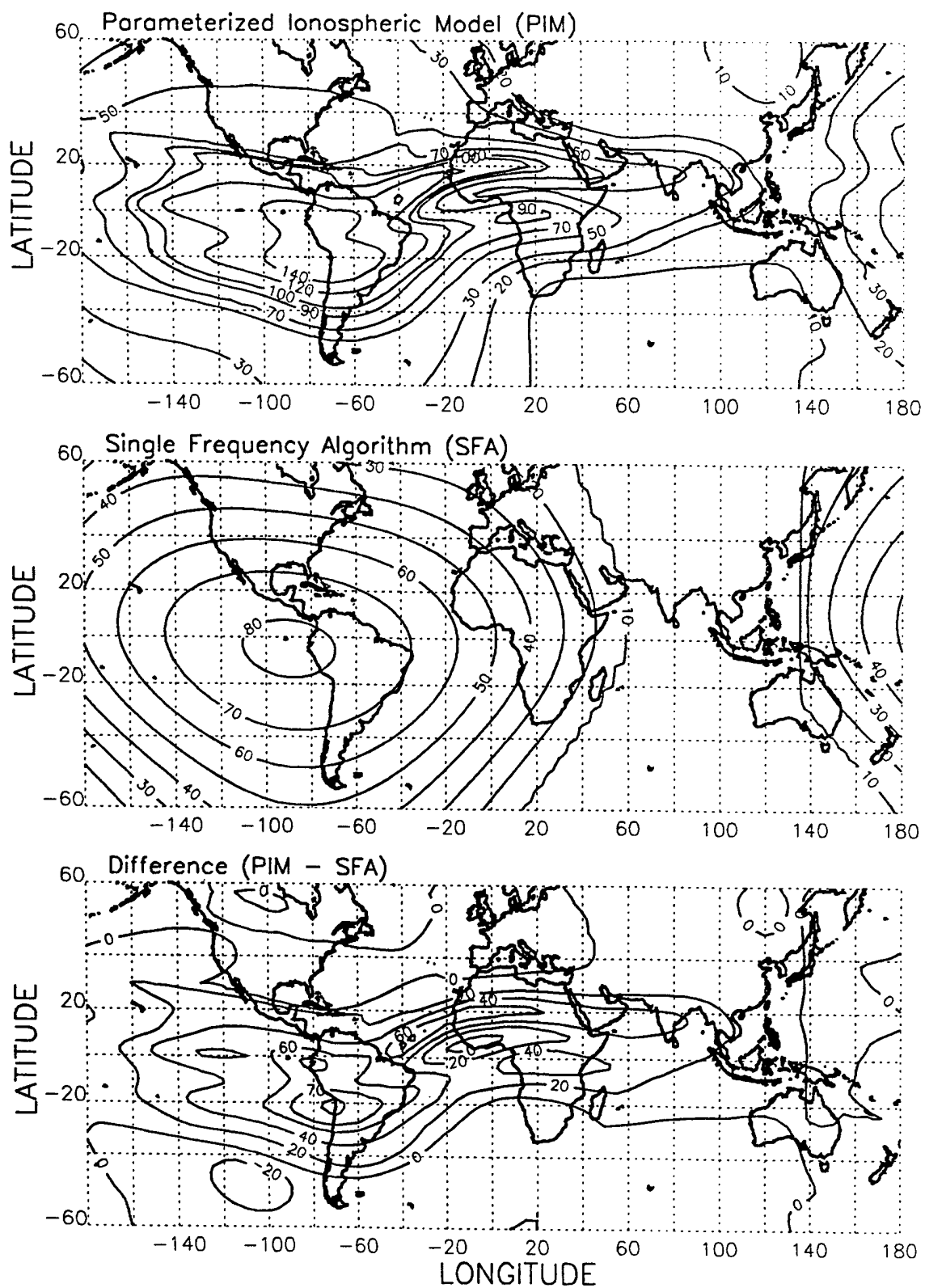
TEC (10^{16} el/m^2)   Solar Maximum/Equinox/20UT

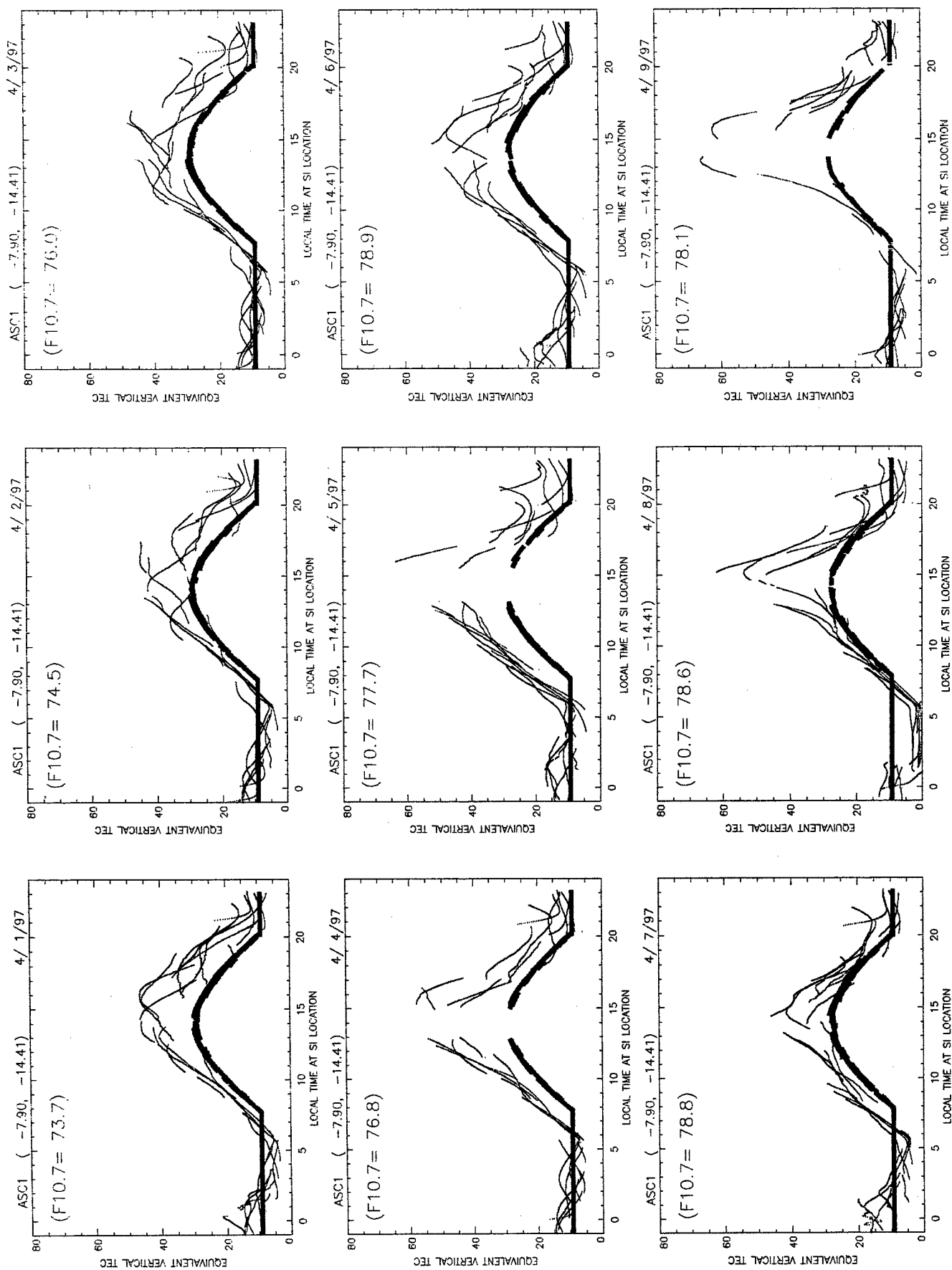**FIGURE 15.** Comparison of PIM TEC Contours and SFA TEC Contours

FIGURE 16. Equivalent Vertical TEC vs Sub-Ionospheric Time   April 1997

27

Next, we extended our research to determine the effects of insufficient ionospheric correction on the actual GPS position calculations. In general, position and time solution accuracy determined by GPS is ultimately expressed as the product of a geometry factor and a pseudo-range error factor. The geometry factor comprises the composite effect of the satellite to user geometry on the GPS solution error. It is generically called the Dilution of Precision (DOP). The pseudo-range error factor is the statistical sum of the contributions from error sources associated with each satellite. Uncorrected ionospheric errors are included in the error sources that are accounted for in the pseudo-range error factor. In our efforts, we have coordinated work with staff members at AFRL to determine the actual error in position calculations caused by inaccurate ionospheric corrections for single-frequency GPS users. First, we utilized GPS satellite ephemerides to determine the best geometry that created optimal DOP values over the entire globe. These satellite specifications were then input to the PIM model to simulate a dual-frequency TEC measurement. Single-frequency estimates of TEC were simultaneously generated from the in-house single-frequency user algorithm. The difference between the dual-frequency TEC measurements from PIM and the single-frequency TEC measurements were then used as errors to the pseudo-range error factor for each satellite. Errors in positioning were then estimated for the single-frequency GPS user worldwide. Figure 17 illustrates the first results from this effort. This figure shows errors reaching 12 meters in the equatorial anomaly region at approximately 1100 hours UT for a quiet ionosphere during a solar moderate period.

The next step in this work will to be to calculate the horizontal and vertical locations using the near-real-time dual-frequency GPS measurements that are provided by JPL for 24 widely spaced GPS stations. Similar to the work described above, we would compare these calculations to those obtained with the single frequency ionospheric correction algorithm. This step will serve to validate our previously modeled measurements and to provide a prototype for a near-real-time model of PLGR navigation errors induced by uncorrected ionospheric delay.

3. OBSERVATIONAL DATABASES

3.1. Spatial and Temporal Variations in Ionospheric Range Delay

Work has continued in the determination of the spatial and temporal variations in ionospheric range delay. This study is based on dual-frequency GPS measurements recorded from 1993 through early 1997. GPS measurements provide the unique opportunity to observe simultaneous ionospheric estimates in up to eight different slant paths from a single receiver. From these measurements, one can infer the spatial variations viewed from one location. In addition, the temporal variation in range delay at a single location can be made by determining the rate of change in the ionosphere as measured with the highest elevation satellite at particular times of day.

This analysis is intended to provide a characterization of the ionospheric variations that will be encountered in the Federal Aviation Administration's (FAA) operational Wide Area Augmentation System (WAAS). The WAAS system is expected to experience the most problems during periods of ionospheric scintillation and during periods of major geomagnetic storms activity when the spatial and temporal gradients in the ionosphere can be higher than
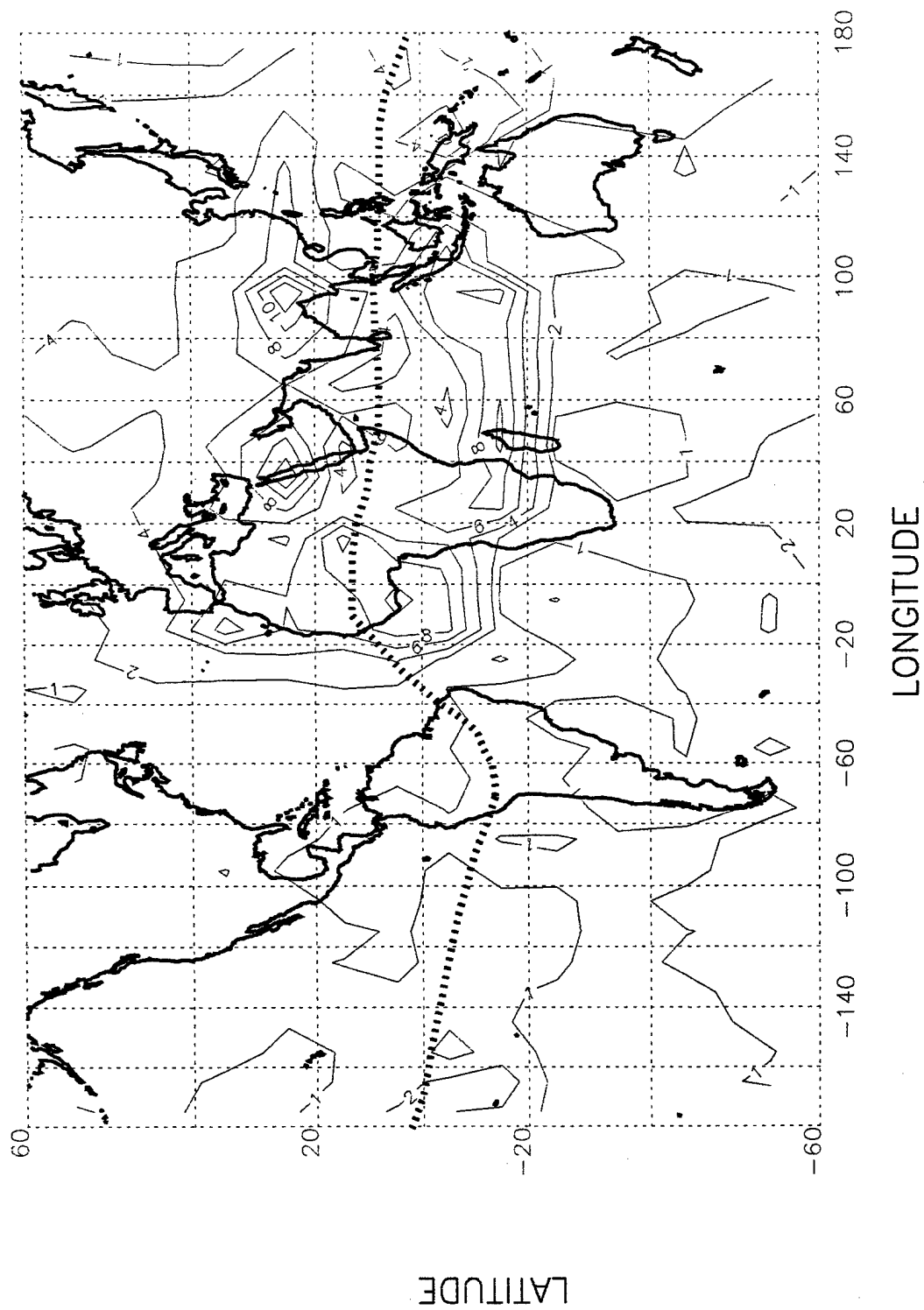
28

FIGURE 17. Ionospheric 3D Error (m) April 10, 1998 11:15 UT

usual. This study will be performed to quantify the magnitude and frequency of these large spatial and temporal gradients.

For this work, we obtained and processed GPS data for June and September of 1994 and for January, March, June and September of 1995 at the following sites:

> Westford, Massachusetts
> Goldstone, California
> Albert Head, British Columbia
> Fairbanks, Alaska
> Kokee, Hawaii.

A statistical analysis has been performed on the temporal variations in range delay recorded at these stations. The statistics are based on the rate of change in range delay for particular times of day at each receiver location. The general conclusion from this analysis is that temporal changes in the mid-latitude ionosphere were normally distributed and did not exceed .1 meters/minute during the solar minimum and solar moderate equinox periods. These statistics are well within the estimated physical limits for temporal changes in the WAAS system. It is expected that rates of change will increase during magnetically disturbed periods and during solar maximum. Measurements made closer to the auroral zone at Albert Head, Canada exhibited larger short-term rates of changes that reached 0.4 meters/minute below the 1 percent probability level and are closely related to geomagnetic disturbance. The largest changes in range delay seen over a 1-minute period were recorded at Fairbanks, a station located very close to the auroral region. Rates of change near 0.7 meters/minute were shown to occur at Fairbanks during the solar moderate equinox period. These large variations occurred approximately 2 percent of the time and were also closely related to geomagnetic disturbances. Measurements recorded north of the equatorial anomaly region in Hawaii also exhibited large deviations from a normal distribution and were more affected by variations in the equatorial electrojet than by magnetic activity. The magnitude for 1-minute rates of change for March 1993 at the Hawaii site reached 0.4 meters/minute at the 1 percent probability levels. Note that these results were limited to solar minimum and moderate periods and that higher magnitudes of short-term changes in ionospheric range delay are expected for solar maximum.

3.2. GPS Satellite and Receiver Bias Calculations

One of the limiting factors in using dual-frequency GPS to provide accurate measurements of the ionospheric electron content is the assessment of the differential L2-L1 biases in both the satellite and receiver hardware. The measurement of ionospheric TEC from dual-frequency GPS satellites is derived from the differential group delay of the L1 and L2 signals. The measured differential L2-L1 group delay, however, contains not only the differential delay induced from the ionosphere, but also the differential delays from the satellite and receiver hardware. In order to make absolute measurements of TEC, these satellite and hardware biases must be estimated and removed from the GPS differential group delay measurement.

We have initiated efforts to develop a new algorithm to calculate the combined satellite and receiver biases from GPS data. The algorithm is based on modeling the ionosphere over a 24-hour period with data recorded from one ground location. In this algorithm, the measurements

are used to estimate, in a least square sense, the modeling parameters and biases. Continued efforts are planned to compare our results with results from other algorithms currently in use and to extend the algorithm to include simultaneous measurements from more than one receiver.

3.3. Airglow Data

This effort is focused on testing the Beta Test version of the Auric 1.0 model developed by Computational Physics, Inc. Whether the final version of the model will differ from this beta version will depend on the results obtained in comparison with experimental data by groups such as ours. In comparison to the previous version, the DAYCHEM program in Auric 1.0 is considerably longer indicating that more chemical reactions have been included. Also, in initial comparisons of model and data, the Lyman alpha comparison is better than in the previous model. The 1304 and 1356 oxygen lines in the new version are stronger than in the older model.

We have compared Auric 1.0 with our data from the STS-39 Shuttle flight. On this flight, the spectral data from 1100Åto 1800Å were taken with a viewing angle of 180°. At this viewing angle, the comparison of daytime data and model appears to be fairly good. The comparison with measurements taken at night was also made using the Niteglo program. As expected, the night results are very different from the day results. Agreement between data and model is very good for the Lyman radiation but not so good for the oxygen 1304Å and 1356Å radiations. We are now examining the Niteglo program, especially the excitation rates for the 1304Å and 1356Å radiations.

Comparisons involving the data obtained on Shuttle flight STS-4 have begun. Examples of the results are given in Figures 18 and 19. They are of two types: tangent altitude results (Figure 18) and spectral results (Figure 19). In the tangent altitude results, the intensity of the radiation measured at a given wavelength is plotted as a function of tangent altitude along with the model results. In the spectral results, the intensities of data and model are plotted as a function of wavelength from 1150Å to 1700Å. On the spectral results, we also have the 10-counts data as a function of wavelength. We note that some of the data recorded were as low as one count or less.

We have now reached the point where we are ready to run all the data for the STS-4 and STS-39 flights.

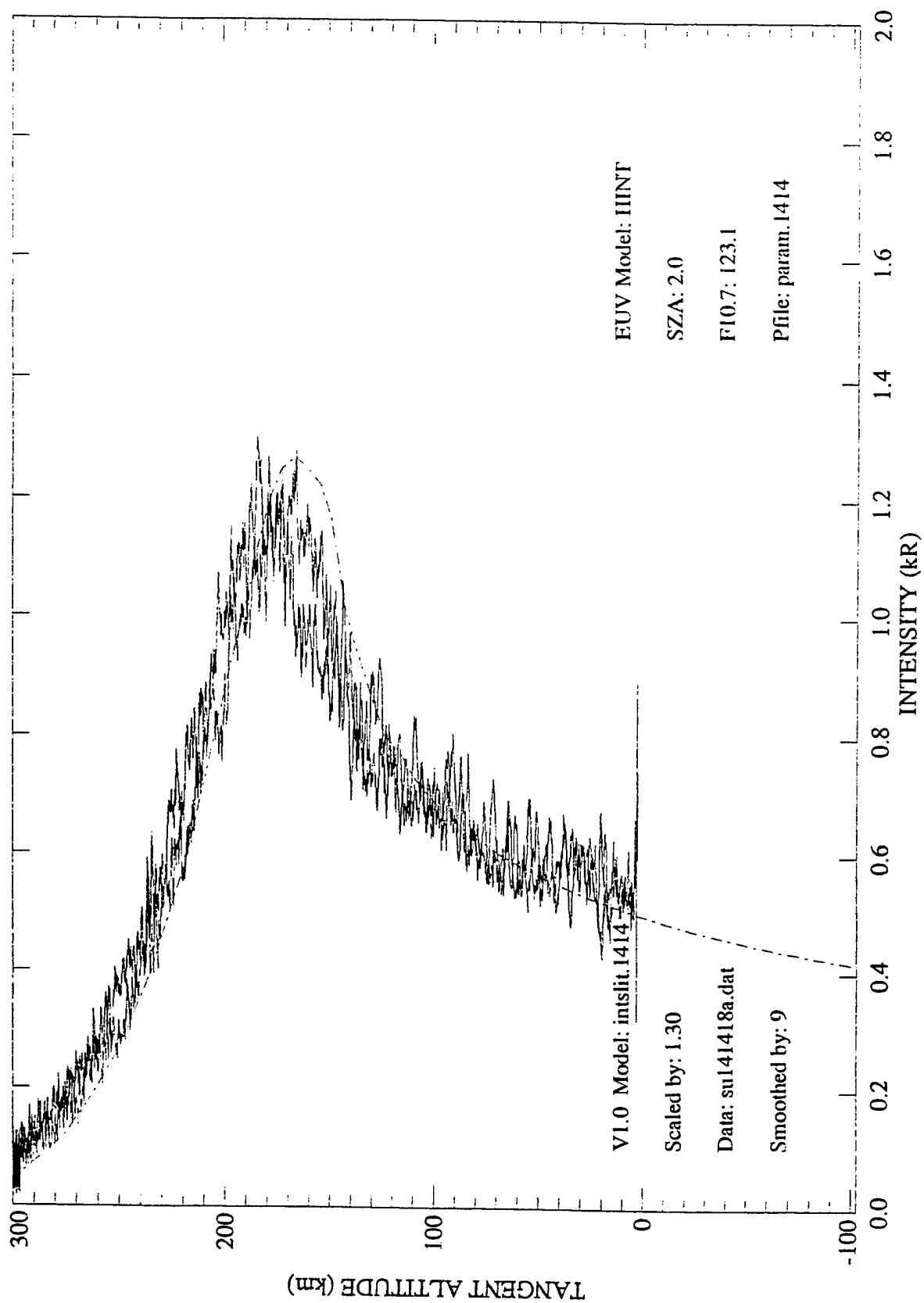**FIGURE 18.** Integration Centered At 1409.0 A

EUV Model: IIINT

SZA: 2.0

F10.7: 123.1

Pfile: param.1414

V1.0 Model: intslit.1414

Scaled by: 1.30
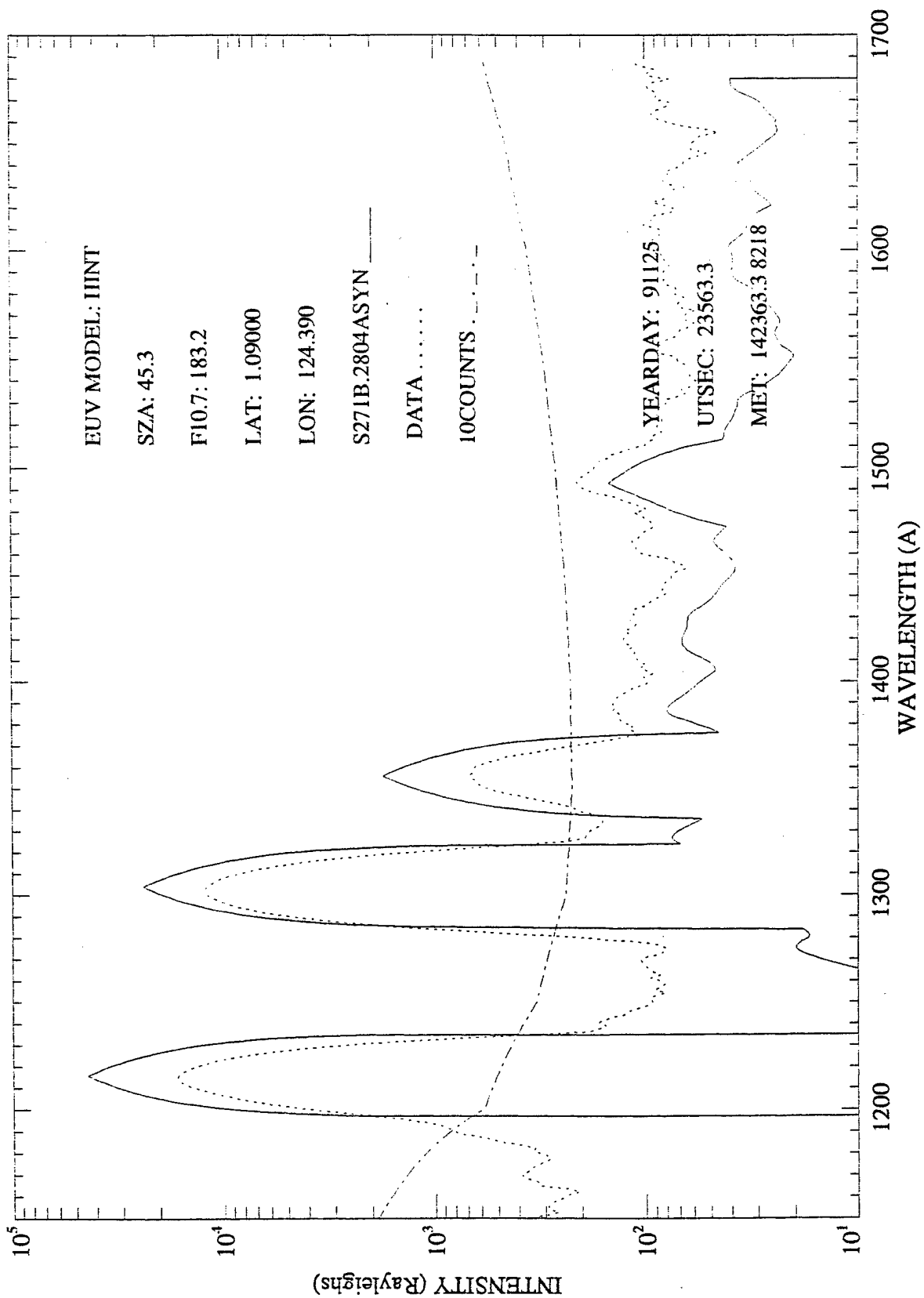
Data: su141418a.dat

Smoothed by: 9

FIGURE 19. HUP STS-4 Spectrum S271B.2804A & Auric Model

4. REFERENCES

Anderson, D.N., D.T. Decker, and C.E. Valladares, Modeling boundary blobs using time varying convection, *Geophys. Res. Lett., 23,* 579-582, 1996.

Basu, S., Su. Basu, J.J. Sojka, R.W. Schunk, and E. MacKenzie, Macroscale modeling and mesoscale observations of plasma density structures in the polar cap, *Geophys. Res. Lett., 22,* 881-884, 1995.

de la Beaujardiere, O., J.D. Craven, V.B. Wickwar, G. Caudal, J.M. Holt, L.A. Frank, L.H. Brace, D.S. Evans, and J.D. Winningham, Universal time dependence of nighttime F region densities at high latitudes, *J. Geophys. Res., 90,* 4319-4332, 1985.

Hajj, G.A., and L.J. Romans, Ionospheric mapping with the GPS/MET, *Proceedings of the Institute of Navigation 52nd Annual Meeting,* pp. 539-545, 1996.

Hoeg, P., A. Hauchecorne, G. Kirchengast, S. Syndergaard, B. Belloul, R. Leitinger, W. Rothleitner, Derivation of atmospheric properties using radio occultation technique, DMI Scientific Report 95-4, Danish Meteorological Institute, 1995.

Pryse, S.E., L. Kersley, and I.K. Walker, Blobs and irregularities in the auroral ionosphere, *J. Atmos. Terr. Phys., 58,* 205-215, 1996.

Rino, C.L., R.C. Livingston, R.T. Tsunoda, R.M. Robinson, J.F. Vickrey, C. Senior, M.D. Cousins, J. Owen, and J.A. Klobuchar, Recent studies of the structure and morphology of auroral zone F region irregularities, *Radio Sci., 18,* 1167-1180, 1983.

Tsunoda, R.T., High-latitude F region irregularities: A review and synthesis, *Rev. Geophys., 26,* 719-760, 1988.

Vickrey, J.F., C.L. Rino, and T.A. Potemra, Chatanika/TRIAD observations of unstable ionization enhancements in the auroral F-region, *Geophys. Res. Lett., 7,* 789-792, 1980.

Weber, E.J., R.T. Tsunoda, J. Buchau, R.E. Sheehan, D.J. Strickland, W. Whiting, and J.G. Moore, Coordinated measurements of auroral zone plasma enhancements, *J. Geophys. Res., 90,* 6497-6513, 1985.

5. PRESENTATIONS

We were involved in 12 presentations at various scientific meetings. There are also two presentations that have been submitted to the Spring AGU meeting that is being held in May 1998.

- D.T. Decker, P.H. Doherty, and D.N. Anderson, "Modeling the Low Latitude F Region Weather" presented at the SWIFT workshop, CEDAR meeting, held in June 1997 in Boulder, Colorado.

- D.T. Decker, C.E. Valladares, E. MacKenzie, D.N. Anderson, S. Basu, and Su. Basu, "Modeling the Climatology and Weather of Large-Scale Plasma Structures in the High Latitude F Region", presented at the Third Joint Workshop for CEDAR HLPS/GAPS held at in Peaceful Valley, Colorado, June 15-17, 1997.

Abstract

Observations have shown that much of the high latitude F-region weather is caused by small scale (irregularities) and large scale electron density structures. These same observations also suggest that there is an intimate cause and effect relation between the large scale structures (>10 km) and the smaller scale (<10 km) irregularities. This, in turn, implies that understanding the large scale F-region structures is a key starting point for understanding the F-region weather at both small and large scales. Theoretical work on modeling large scale structures has recently demonstrated that we can simulate the formation and evolution of polar cap patches and boundary blobs, two types of F-region structures that are observed coincident with smaller scale irregularities. However in general, it has not been demonstrated that on a given day with inputs specific to that day that we can accurately specify where and when such structures will appear. In this paper, we will discuss ongoing efforts towards developing this capability.

Our ability to model polar cap patches has been steadily evolving over the last decade. The early theoretical work on how patches might be created focused on studying a few convection trajectories as a first step at modeling various patch producing mechanisms. *Sojka and Schunk* [1986] showed that spatially limited regions of cusp/cleft precipitation could easily produce factor of 2 enhancements in density that were then transported across the nighttime polar cap. *Anderson et al.* [1988] found that a sudden change in the size and strength of the global convection pattern could create a sevenfold enhancement in the F_2 peak density (N_mF_2) at Thule, Greenland. *Sojka and Schunk* [1988] demonstrated theoretically that large electric fields could create regions of density depleted by a factor of 4. The first simulations of the entire polar cap that actually created patch-like structures in the polar cap were performed by *Sojka et al.,* [1993a]. In this study, simulations were performed that used simple time-varying global convection to produce density structures that were indistinguishable from patches. This was followed by *Decker et al.* [1994] using six different global convection patterns and localized velocity structures to reproduce digisonde measurements made at Sondrestrom, Greenland. Building on these successes, *Sojka et al.* [1994] used time varying convection to simulate the seasonal and UT dependence of patches and predicted a morphology that was consistent with observations of *Buchau et al.* [1985]. More recently, *Valladares et al.* [1996] has simulated the effects of large plasma jets along with a background poleward convection to produce patch like structures similar to what was observed by the Sondrestrom incoherent scatter radar on February

19, 1990. *Bowline et al.* [1996] performed several simulations for various IMF B_y orientations. From these simulations they predicted the B_y dependence of patches at different ground-based sites and found that the results for Sondrestrom and NyAlesund are qualitatively consistent with digisonde observations. Finally in another recent paper, *Basu et al.* [1995] demonstrated that the simulated seasonal and UT variation of polar cap patches has a "remarkable similarity" to the observed behavior of satellite signal scintillations.

In contrast to patches, much less theoretical work has been done on blobs. While these regions of enhanced plasmas that are seen in the auroral F region have been categorized into several types and a variety of sources have been postulated, most work has been observational and only a few theoretical efforts have been reported [*Robinson et al.,* 1985; *Anderson et al.,* 1996]. In the recent work of *Anderson et al.* [1996] the Global Theoretical Ionospheric Model (GTIM) was used to study one mechanism for producing boundary blobs. Using time-dependent convection patterns, it was found that polar cap patches can be convected out of the polar cap and swept sunward by the dusk convection cell. The resulting structures had many of the features associated with boundary blobs. However, the simulations were not designed to produce blobs in any particular auroral region or at any particular time. In the first part of this paper, we report on our efforts to produce blobs observed on a specific day by the Chatanika radar and on our efforts to compare theoretical blob morphology to observed scintillation morphology. *Weber et al.* [1985] documented Chatanika radar observations of boundary and sub-auroral blobs from 0543 to 1213 UT on 29 January 1979. We have simulated this day by temporally varying the ionospheric convection input to the model. We find that blobs can be produced over the latitudes and time sector observed by Chatanika. Since we know little about the actual convection on that day, we have not modeled the observations in detail. Rather these simulations illustrate that time-varying convection is capable of producing blobs at the times and locations that they are observed.

As in the case of patches, we can also use time-varying convection to simulate the seasonal and UT dependence of blobs. The validation of such results, however, is hampered by the fact that blobs are an auroral phenomenon and no single ground station can be used as the sole source of observed blob morphology. Further, while blobs have been observed at several locations, we know of no assembled data set that gives the complete seasonal and UT morphology of blobs. Our approach is to perform a study similar to *Basu et al.* [1995] and compare simulated blob morphology to 250-MHz intensity scintillation observations made at a particular location (Sondrestrom). As we are using data from a single station we are restricting the times considered to 20 to 8 UT. The comparisons are between the percentage occurrence of intensity scintillations and the simulated maximum density in a local time slice running through the ionospheric pierce points of the Sondrestrom observations.

While the above studies tell us that time-dependent convection is capable of producing both patches and blobs, many questions remain concerning whether we can accurately specify the appearance of such large scale structures on a given day. To date, for the most part we have either fitted observations by using convection as a free parameter or we have used simple convection patterns to produce climatology. Now, we need to examine the use of inputs specific to a given day for the purpose of specifying that day's patch and blob weather. In particular, we are focusing on two related questions. How well do we need to know the time varying convection pattern and can the formation of large scale plasma structures be understood primarily in terms of time-dependent convection? To begin answering these questions, we have been focusing on the sensitivity of model results to details of the time-varying convection pattern. In

preparation for this study, we have modified GTIM to accept a greater variety of convection patterns. In previous work, we have used convection patterns coming from the works of *Heelis et al.* [1982], *Heppner and Maynard* [1987], and *Hairston and Heelis* [1990]. Over the last several years, other sources have become available including several periods that have been analyzed using the assimilative mapping of ionospheric electrodynamics (AMIE) technique [*Richmond and Kamide,* 1988; *Knipp et al.,* 1991; *Richmond,* 1992; *Knipp et al.,* 1993], the

IZMIRAN electrodynamic model (IZMEM) [*Papitashvili et al.,* 1994], the Weimer model [*Weimer,* 1995], and the Goose Bay HF model [*Ruohoniemi and Greenwald,* 1996]. We are also beginning to get potential patterns for specific days based on SuperDARN observations [*Greenwald,* 1995]. Accordingly, GTIM has now been modified to use a convection database from any of these sources of convection potentials.

Our first sensitivity study is a series of simulations using different representations of the convection pattern during a period of changing IMF B_y. The first run uses a steady state Hairston-Heelis pattern, the second uses two Hairston-Heelis patterns, the third uses a series of Weimer patterns driven by IMF, the fourth uses patterns based on actual Super/DARN observations, and the fifth uses the Super/DARN pattern with imbedded vortex-like velocity structures. The results of these simulations will be compared at various ground locations in the high latitude regions. Our goal is to see how the simulated ionospheres change at various locations as we go from the simple and unrealistic steady state convection pattern to a pattern that varies every two minutes and includes mesoscale velocity structures.

Anderson, D.N., J. Buchau, and R.A. Heelis, Origin of density enhancements in the winter polar cap ionosphere, *Radio Sci., 23,* 513, 1988.

Anderson, D.N., D.T. Decker, and C.E. Valladares, Modeling boundary blobs using time varying convection, *Geophys. Res. Lett., 23,* 579-582, 1996.

Basu, S., Su. Basu, J.J. Sojka, R.W. Schunk, and E. MacKenzie, Macroscale modeling and mesoscale observations of plasma density structures in the polar cap, *Geophys. Res. Lett., 22,* 881-884, 1995.

Bowline, M.D., J.J. Sojka, and R.W. Schunk, Relationship of theoretical patch climatology to polar cap patch observations, *Radio Sci., 31,* 1996.

Buchau, J., E.J. Weber, D.N. Anderson, H. C. Carlson, Jr., J.G. Moore, B.W. Reinisch, and R.C. Livingston, Ionospheric structures in the polar cap: Their origin and relation to 250-MHz scintillation, *Radio Sci., 20,* 325, 1985.

Decker, D.T., C.E. Valladares, R. Sheehan, Su. Basu, D.N. Anderson, and R.A. Heelis, Modeling daytime F layer patches over Sondrestrom, *Radio Sci., 29,* 249-268, 1994.

Greenwald, R.A. et al., DARN/SuperDARN: A global view of the dynamics of high-latitude convection, *Space Sci. Rev., 71,* 761-796, 1995.

Hairston, M.R. and R.A. Heelis, Model of the high-latitude ionospheric convection pattern during southward interplanetary magnetic field using DE-2 data, *J. Geophys. Res., 95,* 2333, 1990.

Heelis, R.A., J.K. Lowell, and R.W. Spiro, A model of the high-latitude ionospheric convection pattern, *J. Geophys. Res., 87,* 6339, 1982.

Heppner, J.P. and N.C. Maynard, Empirical high-latitude electric field models, *J. Geophys. Res., 92,* 4467, 1987.

Knipp, D.J., A.D. Richmond, B. Emery, N.U. Crooker, O. de la Beaujardiere, D. Evans, and H. Kroehl, Ionospheric convection response to changing IMF direction, *Geophys. Res. Lett., 18,* 721, 1991.

Knipp, D.J., B.A. Emery, A.D. Richmond, N.U. Crooker, M.R. Hairston, J.A. Cumnock, W.F. Denig, F.J. Rich, O. de la Beaujardiere, J.M. Ruohoniemi, A.S. Rodger, G. Crowley, B.-H. Ahn, D.S. Evans, T.J. Fuller-Rowell, E. Friis-Christensen, M. Lockwood, H.W. Kroehl, C.G. Maclennan, A. McEwin, R.J. Pellinen, R.J. Morris, G.B. Burns, V. Papitashvili, A. Zaitzev, O. Troshichev, N. Sato, P. Sutcliffe,

and L. Tomlinson, Ionospheric convection response to slow strong variation in a northward interplanetary magnetic field: A case study for January 14, 1988, *J. Geophys. Res., 98,* 19,273, 1993.

Papitashvili, V.O., B.A. Belov, D.S. Faermark, Ya.L. Feldstein, S.A. Golyshev, L.I. Gromova, and A.E. Levitin, Electric potential patterns in the northern and southern polar regions parameterized by the interplanetary magnetic field, *J. Geophys. Res., 99,* 13,251, 1994.

Richmond, A.D., Assimilative mapping of ionospheric electrodynamics, *Adv. Space Res., 12,* 59, 1992.

Richmond, A.D. and Y. Kamide, Mapping electrodynamic features of the high-latitude ionosphere from localized observations: technique, *J. Geophys. Res., 93,* 5741, 1988.

Robinson, R.M., R.T. Tsunoda, and J.F. Vickrey, Sources of F region ionization enhancements in the nighttime auroral zone, *J. Geophys. Res., 90,* 7533-7546, 1985.

Ruohoniemi, J.M. and R.A. Greenwald, Statistical patterns of high-latitude convection obtained from Goose Bay HF radar observations, *J. Geophys. Res.,101,* 21,743-21,763, 1996.

Sojka, J. J. and R. W. Schunk, A theoretical study of the production and decay of localized electron density enhancements in the polar ionosphere, *J. Geophys. Res., 91,* 3245, 1986.

Sojka, J.J. and R.W. Schunk, A model study of how electric field structures affect the polar cap F region, *J. Geophys. Res., 93,* 884, 1988.

Sojka, J.J., M.D. Bowline, R.W. Schunk, D.T. Decker, C.E. Valladares, R. Sheehan, D.N. Anderson, and R.A. Heelis, Modeling polar cap F region patches using time varying convection, *Geophys. Res. Lett., 20,* 1783-1786, 1993a.

Sojka, J.J., R.W. Schunk, M.D. Bowline, and E.J. Weber, Model-observation comparisons that show the polar cap patch UT dependence in winter, *EOS, 74,* 94, 1993b.

Sojka, J.J., M.D. Bowline, and R.W. Schunk, Patches in the polar ionosphere: UT and seasonal dependence, , *J. Geophys. Res., 99,* 14,959-14,970, 1994.

Valladares, C.E., D.T. Decker, R. Sheehan, and D.N. Anderson, Modeling the formation of polar cap patches using large plasma flows, *Radio Sci., 31,* 573-593, 1996.

Weber, E.J., R.T. Tsunoda, J. Buchau, R.E. Sheehan, D.J. Strickland, W. Whiting, and J.G. Moore, Coordinated measurements of auroral zone plasma enhancements, *J. Geophys. Res., 90,* 6497-6513, 1985.

Weimer, D.R., Models of high-latitude electric potentials derived with a least-error fit of spherical harmonic coefficients, *J. Geophys. Res., 100,* 19,595, 1995.

- D.T. Decker, C.E. Valladares, and D.N. Anderson, "Specifying the High Latitude F Region Weather" presented at the IAGA meeting held in Uppsala, Sweden in August 1997.

Abstract

Observations have shown that much of the high latitude F-region weather is caused by small scale (irregularities) and large scale electron density structures. These same observations also suggest that there is an intimate cause and effect relation between the large scale structures (>10 km) and the smaller scale (<10 km) irregularities. Theoretical work on modeling large scale structures has recently demonstrated that we can simulate the formation and evolution of polar cap patches and boundary blobs, two types of F-region structures that are observed coincident with smaller scale irregularities. However, it has not been demonstrated that we can accurately model such structures at a particular place and time. In this paper, we report on efforts to use the Global Theoretical Ionospheric Model (GTIM) to determine what is required to accurately specify the appearance of patches and blobs. We will particularly focus on the sensitivity of model results to details of the time-varying convection pattern and the need for a weather specification of the high latitude electric field.

- D.N. Anderson, D.T. Decker, P.H. Doherty, and M.W. Fox, "Modeling the Low Latitude F Region Weather" presented at the 1997 IAGA meeting held in Uppsala, Sweden in August, 1997.

Abstract

The low latitude F-region is known as a very dynamic region where dramatic plasma irregularities can occur over a large range of scale sizes and amplitudes. However, it is also a

region where the ambient F-region plasma has great day-to-day variability. In large part, this variability comes from the day-to-day behavior of the F-region electric field, in particular the zonal field (vertical drift). This is so because the vertical drift is a key factor in determining the basic character of the low-latitude F region. Thus, a primary requirement for modeling the low latitude space weather will be the ability to monitor the electric field and use it as a weather input to an ionospheric model. In this work, we are examining several observational sources (radar, digisonde, and magnetometer) for the day-to-day behavior of the vertical drift and will be using the resultant drifts as inputs to the Global Theoretical Ionospheric Model (GTIM). The usefulness of these sources will be judged by comparisons between GTIM results and various ionospheric measurements such as digisonde, radar, GPS, and TOPEX observations.

- D.T. Decker, C.E. Valladares, E. MacKenzie, D.N. Anderson, S. Basu, and Su. Basu, "Modeling the Climatology and Weather of Blobs", presented at the 1997 IAGA meeting held in Uppsala, Sweden in August, 1997.

Abstract

Over the last 30 years, observations have shown that the auroral F region contains mesoscale structures known as blobs. While these regions of enhanced plasmas have been categorized into several types and a variety of sources have been postulated, most work has been observational and only a few theoretical efforts have been reported [Robinson et al., 1985; Anderson et al., 1996]. In the recent work of Anderson et al. [1996] the Global Theoretical Ionospheric Model (GTIM) was used to model the formation of boundary blobs using time varying convection. The structures produced had many of the features associated with boundary blobs. However, the next step is to demonstrate that both the general climatology of blobs can be modeled and that blobs in a particular region at a particular time can be modeled. We will report on efforts to compare theoretical blob morphology to observed scintillation morphology and first efforts to reproduce blobs observed on a specific day by the Chatanika radar. Discussion will focus on the global observations needed to provide the model inputs as well as the observations with which to constrain the model outputs.

Anderson, D.N., D.T. Decker, and C.E. Valladares, Modeling boundary blobs using time varying convection, *Geophys. Res. Lett.*, *23*, 579-582, 1996.

Robinson, R.M., R.T. Tsunoda, and J.F. Vickrey, Sources of F region ionization enhancements in the nighttime auroral zone, *J. Geophys. Res.*, *90*, 7533-7546, 1985.

- P.H. Doherty, R. Loh, and D.N. Anderson, "Statistics of the Spatial and Temporal Variations in Ionospheric Range Delay", presented at ION-GPS 97 held in Kansas City, Missouri in September 1997. It also appeared in the *Proceedings of the ION 53rd Annual Meeting, 1997*.

Abstract

In this study, we present the statistics of the spatial and temporal variations in ionospheric range delay recorded at several locations in the continental US, Canada, Alaska and Hawaii. These measurements, recorded from 1993 through early 1997, were obtained from the International GPS Geodynamics Service (IGS) network, managed by the Jet Propulsion Laboratory. The statistics of spatial variations are based on simultaneous measurements made along different lines of sight at each location. Statistics of the temporal ionospheric variations are based on the highest elevation measurement at particular times of day at each individual

receiver location. Since these measurements cover only solar moderate to minimum conditions, we augment the statistics on the temporal variations with a historical data base of ionospheric measurements recorded at similar locations over a full solar cycle. The historical data is based on Faraday rotation measurements of VHF signals from geostationary satellites of opportunity. Unfortunately, the sites included in the historical data are too widely spaced to infer spatial variations in the next solar maximum.

This analysis is intended to provide a characterization of ionospheric variations that will be encountered in the Federal Aviation Administration's (FAA) operational Wide Area Augmentation System (WAAS). The WAAS system is intended to support en-route and precision-approach flight operations. An important factor in the operational system will be the accuracy of the vertical ionospheric delay estimates that will be provided to a user aircraft in a satellite broadcast message. These estimates of vertical ionospheric delay will be based on slant dual-frequency GPS measurements of ionospheric range delay made at 24 reference stations (21 in the continental US, 1 in Hawaii, 1 in Alaska and 1 in Puerto Rico). Historically, the ionosphere has proved to be extremely variable in nature. Its behavior is a function of geographic location, local time, season, geomagnetic activity and solar activity. In the continental US, measurements of ionospheric range delay at midday can range from less than 2 meters at solar minimum to nearly 20 meters at solar maximum. In Hawaii, daytime observations of range delay as high as 30 meters have been recorded during a solar maximum period. Fortunately, these large variations in the ionosphere develop slowly as a function of long term changes in solar activity and are not likely to cause degraded accuracy in the vertical ionospheric delay estimates for WAAS. The most critical problems of ionospheric estimation for WAAS will occur during periods of ionospheric scintillation and during periods of major geomagnetic storm activity when the spatial and temporal gradients in the ionosphere can be significantly higher than usual. This study will quantify the magnitude and frequency of these large spatial and temporal gradients observed with dual-frequency GPS from single locations during solar moderate to minimum periods. It will also provide a historical reference to the temporal gradients observed during a previous solar maximum period.

• P.H. Doherty, M.C. Smitham, D.N. Anderson, G.J. Bishop, and A.J. Mazzella, "Ionospheric Effects on Single Frequency GPS Positioning", presented at to the Space Weather Effects on Propagation of Navigation and Communication Signals held in Bethesda, Maryland in October 1997.

Abstract

The ionosphere remains one of the largest and most variable sources of error for GPS positioning and navigation. Dual-frequency GPS users acquire highly accurate estimates of ionospheric range delay from the differential group delay and phase advance measurements made at the two GPS frequencies of 1.6 and 1.2 GHz. Single-frequency users, however, are limited to

a less accurate ionospheric correction that is calculated with the current GPS ionospheric correction algorithm. This single-frequency user algorithm was developed in the mid-1970's to correct for approximately 50 percent of the total ionospheric range error. This level of correction may be acceptable to most users of single-frequency GPS; however, it is not suitable for users who require a high degree of accuracy.

The U.S. Department of Defense (DoD) has procured over 100,000 Precision Lightweight GPS Receivers (PLGR) to provide precise time and positioning to troops in the field. The PLGR is a single-frequency receiver that is equipped with a cryptographic key to counteract the effects of selective availability (the intentional degradation of GPS signal accuracy). The largest remaining source of error for the PLGR is the ionosphere.

In this presentation, we will discuss a research task that is intended to satisfy a DoD request to provide near real-time information on the magnitude of the positioning errors which the single-frequency PLGR GPS receiver experiences due to uncorrected ionospheric effects. The ultimate goal of this task is to provide the capability to generate regional and global maps of these positional errors in near real-time. This product will utilize the near real-time measurements of TEC that are currently provided to the 55th Space Weather Squadron by the Ionospheric Measuring System (IMS) and the Jet Propulsion Laboratory. The maps generated by the final product will be a useful measure of when and where the ionosphere is the limiting factor to navigation and positioning for both DoD and non-DoD single-frequency GPS users.

- D.N. Anderson, D.T. Decker, and P.H. Doherty, "Simulations of GPS/MET Ionospheric Observations", presented at the Workshop on Ionospheric Determination and Specification for Ocean Altimetry and GPS Surface Reflections held in Pasadena, California, December 1997.

Abstract

GPS/MET is a program using a low earth-orbiting satellite instrumented with a dual-frequency GPS receiver to perform limb soundings of the atmosphere using radio occultation of GPS satellites. The primary purpose of the program is to perform remote sensing of the troposphere and stratosphere. However, the limb viewing geometry does provide a unique opportunity for ionospheric research. The useful measured quantity in this case is the Total Electron Content (TEC) between the low earth-orbiting satellite and a particular GPS satellite. In contrast to ground-based GPS measurements, the limb-viewing geometry can provide the type of vertical information that is poorly measured by ground-based GPS measurements.

In this paper, the Parameterized Ionospheric Model (PIM) is used to simulate the TEC as observed by the GPS/MET low earth-orbiting satellite. PIM is based on global, theoretical, first principles ionospheric models that calculate electron densities as a function of altitude, latitude, and local time. These models include the effects of production of ionization by solar extreme ultraviolet radiation and electron precipitation; loss through charge exchange with molecular nitrogen and oxygen; and transport by diffusion, neutral winds, and ExB convection drifts. The simulations are designed to assess the feasibility of determining realistic electron density profiles (EDP) from GPS/MET observations. Examples will be given of simulated TEC measurements, inversions of those measurements into EDPs, and comparisons with PIM EDPs. Validations will also be presented involving inversions of actual GPS/MET observations and comparisons with appropriate digisonde measurements.

41

Abstract

The last few decades have seen the development of various regional and global first-principle ionospheric models. These models, which involve solving first-principle equations, have been successfully used to elucidate much of the physics of the ionosphere and to explain the observed ionospheric climatology. However, in recent years, there has been an increased interest in understanding not just the ionospheric climatology but the ionospheric weather. In particular, there is now a National Space Weather Program (NSWP), which has the goal of developing an interagency system that can provide observations, specification, and forecasts of the space environment. In this context, "space weather" refers to conditions on the sun and in the solar wind, magnetosphere, ionosphere, and thermosphere that can influence the performance and reliability of space-borne and ground-based technological systems and can endanger human life or health. Given the ionosphere's role as a link in the "trail of energy flow" from the sun to Earth and as a region where many adverse effects can occur, there has been a growing effort towards developing ionospheric physics-based models into first-principle ionospheric weather models. This review will discuss these efforts to develop weather models from what have essentially been climatological first-principle models. In particular, the focus will be on the ionospheric F region and the fluid models appropriate for that region. Discussion will include definitions of ionospheric weather, the modeling approaches being used to produce that weather, examples of weather modeling for the low-, mid- and high-latitude regions of the ionosphere, and developments needed for satisfying the goal of the NSWP.

- P.H. Doherty, J.A. Klobuchar, and J. Aarons, "An Overview of Ionospheric Effects on GPS Signals", presented at the 1998 National Radio Science Meeting held in Boulder, Colorado in January 1998.

Abstract

The Global Positioning System (GPS) provides accurate and continuous position, velocity and time information to users worldwide. The satellites transmit signals on 2 L-band frequencies (L1 at 1.6 GHz and L2 at 1.2 GHz). As the signals propagate from a GPS satellite to a GPS receiver located on or near the Earth, they are modified in a number of ways by their encounter with the total number of electrons (TEC) that comprise the ionosphere. The primary effects that the ionosphere imposes on GPS signals are errors in range and range-rate, signal fading (amplitude scintillation), and loss of carrier phase lock (phase fluctuations). Although these effects are considered a nuisance to most GPS users, they provide the ionospheric research community with a unique ionospheric sensing tool.

In this presentation, we will review how the ionosphere affects GPS signals, how large the effects are and how the effects can be mitigated. In addition, we will discuss the sources of potential errors in making absolute corrections for ionospheric effects. These potential sources of error include the calibration of hardware differential group delay offsets and the conversion of slant TEC measurements to equivalent vertical TEC in the presence of gradients.

One advantage of using GPS is that multi-site, multi-station measurements can be made. The International GPS Geodynamics Service (IGS) network currently supports more than 160 sites located worldwide. In addition, the National Oceanic and Atmospheric Administration (NOAA) coordinates the Continuously Operating Reference Station (CORS) network of approximately 100 sites located nationwide. Each of these networks provide dual-frequency code range and carrier phase data recorded at their sites to users at no cost. This presentation will include a discussion on current studies that utilize the GPS measurements provided by these networks.

One study employs the data to infer the spatial and temporal variations in ionospheric range delay. Other studies include the use of phase fluctuations to characterize the development of ionospheric irregularities in the equatorial and auroral regions.

- D.T. Decker, P.H. Doherty, D.N. Anderson, F.J. Rich, and C. Rocken, "GPS Occultation: A New Remote Sensing Technique for the Ionospheric Topside?", submitted to the 1998 Spring AGU meeting to be held in Boston, Massachusetts in May 1998.

Abstract

GPS occultation refers to an observational technique that uses a low earth orbiting satellite instrumented with a GPS receiver to perform limb soundings of the atmosphere using radio occultation of GPS satellites. An ionospheric quantity that can be measured by this technique is the limb profile of the total electron content (TEC). However, the usefulness of such observations depends in large part on how effectively the TEC limb profiles can be inverted into vertical electron density profiles (EDP). Validation of possible inversion algorithms has focused primarily on their ability to infer the F_2 peak and the bottomside of the EDP. But what is also needed is validation of these algorithms' ability to produce an accurate topside EDP. One possibility is to take advantage of the fact that during solar minimum there are times and locations where the transition from O^+ dominance to H^+ dominance can be below the altitude (~750 km) of the GPS/MET satellite. For those cases, it should be possible to make a prediction about the total density and ion composition in the topside ionosphere. During the lifetime of GPS/MET, DMSP satellites were making ion composition measurements at around 840 km. In this preliminary study, we will compare GPS/MET based predictions with statistical compilations of DMSP composition observations. While this is not as rigorous a test as a one to one comparison between coincident GPS/MET observations and incoherent scatter radar measurements, it does represent an opportunity to determine if a GPS/MET determined topside morphology is consistent with that measured by DMSP.

- J.A. Vladimer, P. Jastrzebski, M.C. Lee, P.H. Doherty, D.T. Decker, and D.N. Anderson, "Longitude Structure of Ionospheric TEC at Low latitude Measured by the TOPEX/Poseidon Satellite", submitted to 1998 Spring AGU meeting to be held in Boston, Massachusetts in May 1998.

Abstract

Longitude structure of ionospheric Total Electron Content (TEC) at low latitudes has been evaluated using the NASA/CNESS* TOPEX/Poseidon satellite. The TEC data set is given by the ionospheric range correction which is computed from TOPEX dual-frequency altimeter measurements. The satellite's orbit allows analysis of vertical-measured TEC values at approximately 30° intervals of longitude across the world at local time differences of only 6 - 12 minutes. Patterns of longitudinal dependence of the equatorial anomaly with respect to amplitude and position were observed during equinox, summer, and winter of 1993, 1994 and 1995. Consistent occurrence of relative maximum anomaly TEC values in the Indian/Asian longitude sector and of relative minimum anomaly TEC values in the Pacific sector exist on a day-to-day basis. This longitude signature of the equatorial anomaly is evaluated in terms of the influences of local time, season, solar cycle and magnetic activity. Anomaly shape and hemisphere symmetry, as well as TEC variability within longitude and latitude bins, are

addressed. PIM and GTIM model results are presented in an attempt to reproduce and validate explanations for the distinctive longitude structure.

* Centre Nationale D'Etudes Spatiales

6. JOURNAL ARTICLES

- R.S. Conker, M.B. El-Arini, T.W. Albertson, J.A. Klobuchar, and P.H. Doherty, "Description and Assessment of Real-Time Algorithms to Estimate the Ionospheric Error Bounds for WAAS", *Navigation, Journal of The Institute of Navigation, 44*(1), Spring 1997.

- Dwight T. Decker, David N. Anderson, and Amanda J. Preble, "Improving IRI-90 Low-Latitude Electron Density Specificatication", *Radio Sci., 32,* 2003-2019, 1997.

- J.A. Vladimer, M.C. Lee, P.H. Doherty, D.T. Decker, and D.N. Anderson, "Comparisons of TOPEX and Global Positioning System Total Electron Content Measurements at Equatorial Anomaly Latitudes", *Radio Sci., 32,* 2209-2220, 1997.

- D.N. Anderson, M.J. Buonsanto, M. Codrescu, D. Decker, C.G. Fesen, T.J. Fuller-Rowell, B.W. Reinisch, P.G. Richards, R.G. Roble, R.W. Schunk, and J.J. Sojka, "Intercomparison of Physical Models and Observations of the Ionosphere", *J. Geophys. Res., 103,* 2179-2192, 1998.